Investigating the Dynamics of Suspended Particulate Matter in the North Sea Using a Hydrodynamic Transport Model and Satellite Data Assimilation

Dissertation

zur Erlangung des Doktorgrades der Naturwissenschaften

im Department Geowissenschaften der Universität Hamburg

vorgelegt von

Mikhail Dobrynin

aus Sankt Petersburg

Hamburg 2009

Als Dissertation angenommen vom Department Geowissenschaften der

Universität Hamburg

auf Grund der Gutachten von Prof. Dr. Hans von Storch

und P.D. Dr. habil. Thomas Pohlmann

Hamburg, den 15. April 2009

Prof. Dr. Kay-Christian Emeis

Leiter des Departments für Geowissenschaften

Summary

Suspended particulate matter (SPM) changes light penetration depth in water and thus is an important component of marine ecosystems in the coastal and shallow regions of the world, i.e. the North Sea. The visible effect of SPM presence in seawater is the change of water color from blue to yellow depending on the SPM concentration under different ambient conditions. This study combines numeric modeling with satellite data assimilation in order to investigate the dynamics of SPM in the North Sea over a time period from 2002 to 2003.

First, a coupled three-dimensional Circulation and Transport Model for Suspended Particulate Matter (CTM-SPM) was designed based on the existing, improved and newly developed modeling routines. CTM-SPM was then applied to calculate the dynamics of SPM in seawater, as well as the dynamics of the fine sediment in the seabed in the southern North Sea. Modeled SPM exchange processes at the seawater-seabed interface, such as resuspension and erosion are forced by the shear stress due to currents and waves. Model results suggest that the role of these two forcing components of the shear stress velocity is different in the shallow and deep regions, as well as during *calm* (from April to October) and *storm* (from October to April) periods. Therefore, this study investigates the relative impact of currents and waves on the horizontal and vertical distributions of SPM and its seasonality in details.

Calculated SPM concentrations in the North Sea for the years 2002 and 2003 are in good agreement with satellite and in-situ observations. The model results reveal two different patterns in the SPM dynamics typical for the calm and for the storm periods. This study explains the origin and evolution of the zones with high SPM concentration in the coastal areas and in the open North Sea. The

results indicate that it is essential to use a coupled circulation and SPM transport model with realistic forcing data with a temporal resolution of < 1 hour and instant values of shear stress velocity in order to resolve the SPM processes of different time scales, for example flash erosion events and long-term transport by currents. Utilization of the instant values of the shear stress velocity leads to the more realistic representation of the exchange processes at the water-seabed interface and to the more convenient comparison between the snap-shot satellite measurements and model results.

Second, newly developed and validated tool for satellite data processing and quality control based on the flags approach was applied for more than 300 ENVISAT MERIS snapshot scenes in order to provide the SPM concentration fields derived from satellite images for the assimilation into the CTM-SPM model. The satellite data was assimilated into the model using the sequential Optimum Interpolation scheme.

This thesis presents the first attempt of continuous satellite data assimilation into an SPM transport model. The results of this study indicate a great potential for the application of satellite optical data in the SPM modeling. Analyses of the model results with and without satellite data assimilation shows that assimilation effects not only SPM concentrations in the whole water column, but also the fine sediment distribution in the seabed. The data assimilation signal remains in the model for several days after assimilation. Also the seasonal averaged distributions of SPM change due to assimilation. Satellite data assimilation improves the horizontal SPM distribution, especially its fine structures in the location of SPM fronts in the German Bight and near the English cliffs.

The concept presented in this study can be used as a basis for continuous calculations of SPM based on the modeling and satellite data assimilation. It can be also employed in operational purposes and in ecosystem modeling.

Contents

List of Figures

List of Tables

Chapter 1

Introduction

1.1 Background

Suspended particulate matter (SPM) is defined as a fine solid inorganic particles of non-biogenic origin suspended in water. SPM in seawater mostly originates from the fine sediment (mud) in the bottom and fluvial inflow. It is classified by the grain size (Wentworth, 1922; Krumbein and Sloss, 1963), referred to as fine sediment fractions. The most abundant are silt ($4 - 63\mu m$) and clay ($< 4\mu m$). There are also larger (and heavier) fractions ($> 63\mu m$), such as sand or gravel. They are rarely eroded from the seabed and rapidly sink back to the sea bottom. On the contrary, the very fine fraction ($< 1\mu m$) remains in suspension in water for a long time.

SPM is an integral and important part of marine systems in the coastal and shallow regions of the world. One of these regions is the North Sea where the combination of specific topography, weather conditions and sources of SPM allows to make the SPM exchange and distribution processes responsible for the major changes in the marine ecosystem. The visible effect of SPM processes is the change of seawater color from blue to yellow (Jonasz and Fournier, 2007) depending on the SPM concentration resulted under different weather conditions. In particular, SPM distribution in the water column influences the plankton primary production by regulating the light penetration depth in seawater (Reid et al., 1990). Furthermore, SPM can absorb and thus transport some human-made contaminants, such

as heavy metals (Haarich et al., 1993), persistent organic pollutants (Ilyina et al., 2006) and radionuclides (Nies et al., 1999). Finally, knowledge about erosion, transport and deposition of fine sediment in morphodynamic systems is necessary for the construction of coastal protection structures, mining of sand and dredging of navigation channels (de Swart and Calvete, 2003).

In recent years, there has been an increasing interest among scientists in modeling the suspended particulate matter (SPM) dynamics. There have been several attempts to reconstruct the SPM dynamics in the North Sea using two-dimensional (ten Brummelhuis et al., 2001) and three-dimensional (Sündermann and Puls, 1990; Pohlmann and Puls, 1994; Puls et al., 1997; Pleskachevsky et al., 2002; Gayer et al., 2006) models with various combinations of forcing and spatial and temporal resolution.

Fine sediment exchange processes at the seabed-water interface, i.e. resuspension, erosion and deposition depend on the degree of turbulent mixing in the near-bottom layer caused by waves and currents, which can be expressed by the shear stress velocity. The SPM processes have stepwise character. In many SPM models they are controlled by threshold values of shear stress velocity. Calculations using averaged in time current velocities and wave parameters smooth and therefore suppress the magnitude of modeled processes governing the distribution of SPM. This results in the decrease of both the SPM seabed-water mass exchange and the role of the seabed as a source of SPM in the model. In order to resolve the stepwise exchange processes of SPM, instant values of shear stress velocities have to be used in calculations. This can be achieved by embedding SPM exchange and transport processes into a three-dimensional circulation model.

Additionally, spatial resolution also plays an important role in modeling SPM dynamics. Comparison of the circulation model output run with the meso-scale (3 km) and large-scale (20 km) horizontal resolution (Pohlmann, 2006) showed that not only the temperature, salinity and density distributions, but also the kinetic energy is strongly affected by the chosen grid resolution. As SPM dynamics is driven by currents, waves and turbulence, it is better reproduced using fine spatial grid resolution. This is particularly important in the shallow and coastal regions where the SPM content is high and SPM dynamics is intensive.

Furthermore, previous modeling studies (e.g. Gayer et al. (2006)) focused only on the discrete time intervals (a few weeks) and did not cover longer time periods. Such calculations do not display details of the seasonality of the SPM dynamics and can not be used for operational purposes or in ecosystem models, where seasonality plays the key role.

Satellite images can capture SPM in the North Sea and reflect phenomena involved in the SPM dynamics, i.e. river plums, coastal and seabed erosion under storm conditions and SPM fronts. Advantages of satellite data, such as high temporal and spatial resolution, continuity and large coverage make them an important data source for data assimilation in the regional SPM transport models. However, satellite data assimilation into a regional model has a list of difficulties connected with retrieving the surface SPM concentration from the satellite signal. The technical restrictions are due to constraints in the processing algorithms, clouds, seabed reflection in shallow regions and the signal penetration depth that depends on SPM concentration.

1.2 Objectives and outline of this study

The main objectives of this study were to:

- Develop and evaluate a modeling tool based on the existing, improved and newly designed routines for continues long-term circulation, waves and SPM dynamics calculations in the North Sea.
- Reproduce the specific dynamics of SPM in the North Sea using this tool, capturing the stepwise character of SPM processes.
- Design and validate a tool for satellite data processing and quality control.
- Develop the SPM satellite data assimilation method.
- Study the effect of satellite data assimilation on the modeled SPM distributions in the North Sea.

This study aimed at answering two major questions:

1. *What is the relative impact of currents and waves on the horizontal and vertical distribution of SPM in the North Sea and its seasonality?*

   SPM exchange processes such as resuspension and erosion on the seawater-seabed interface are forced by the shear stress due to currents and waves. The role of currents and waves component of the shear stress velocity is different in the shallow and deep regions, as well as in stormy and calm seasons.

2. *Can available satellite data of SPM be used for assimilation into an SPM model, and if yes would it improve modeling results?*

   Satellite data is restricted by a number of shortcomings, such as constraints in the processing algorithms, clouds, seabed reflection in shallow regions (see Section 1.1). After processing and quality control, satellite data can be assimilated into the uppermost layer of the model. This will lead to the change in the entire water column SPM distribution, as well as in the fine sediment in the seabed.

This thesis is organized as follows. The detailed description of processes included in the model, model setup, initial and boundary conditions as well as the description of forcing data are included in the Chapter 2. Chapter 3 gives the description of satellite data processing, developed quality control system and data assimilation method. Chapter 4 presents the dynamics of two major forcing factors in the SPM dynamics: currents and waves, as well as the dynamics of shear stress velocity. Model results including annual time series of SPM in water and in the seabed, surface and vertical SPM distributions in water are evaluated and discussed in Chapter 5. The results of model run in data assimilation mode, the effect of satellite data assimilation on the vertical and horizontal modeled SPM distribution including comparison of the model simulations with and without data assimilation, as well as duration of data assimilation signal described and discussed in Chapter 6. The summary of key results, limitations of the method, making a suggestions about improvements of SPM modeling and thoughts for future work are included in final Chapter 7.

Chapter 2

Architecture of the Circulation and Transport Model for Suspended Particulate Matter (CTM-SPM)

Dynamics of SPM involves interactions between the seabed, seawater and fluvial sources of SPM. Therefore, to achieve realistic reproduction of its distribution in time and space, it is necessary to gather these components in a unified modeling concept, as was attempted in this study. This chapter gives a detailed description of processes governing the dynamics of SPM such as circulation, waves and turbulence, fine sediment processes in see water and seabed, and sources of fine sediment, i.e. rivers and cliffs included in the Circulation and Transport Model for Suspended Particulate Matter (CTM-SPM; Section 2.1). The description of model setup for the North Sea, initial and boundary conditions used to force the model are given in Section 2.2.

2.1 Description of processes included in the model

Circulation and Transport Model for Suspended Particulate Matter (CTM-SPM) is a three-dimensional ocean model designed to describe the long-term dynamics of SPM in the North Sea. CTM-SPM consists of three major components.

- The circulation module based on the model HAMSOM (Section 2.1.1).
- The SPM module is adopted from the GKSS-BSH SPM model (Gayer et al., 2006).
- The newly developed fine sediment bioturbation module is based on the diffusion equation (Section 2.1.5).

All modules are embedded in the same code and are integrated with the time step of 5 minutes. This ensures that the SPM dynamics is calculated using the instant values of currents velocity.

SPM in the model is represented by solid and round inorganic particles suspended in seawater. These particles differ in sources and size and are treated in the model as separate fractions with different properties. The SPM-related processes included in the model can be grouped under four categories:

Transport with ocean currents. In seawater SPM is transported by ocean currents via advection and turbulent diffusion (Section 2.1.2).

Vertical processes in the water column. In seawater SPM settles down due to gravitational sinking. It is also transported by vertical components of turbulent diffusion and advection (Section 2.1.3).

Seabed-water exchange processes. The vertical exchange of SPM between the seabed and water at the seabed-water interface takes place in both directions as a result of sedimentation, resuspension and erosion (Section 2.1.4).

Seabed processes. Bioturbation due to vital activity in the bottom is a primary cause for SPM redistribution in the upper sediment (Section 2.1.5).

Differing from the approach used by Gayer et al. (2006), which assumes a constant bioturbation rate, CTM-SPM includes seasonally and spatially variable bioturbation in the seabed.

2.1.1 Ocean circulation model HAMSOM

The three-dimensional, baroclinic, primitive equation model HAMSOM (Hamburg Shelf Ocean Model) includes the equations of motion and continuity, the equation of state for seawater, as well as transport equations for temperature and salinity. The detailed description of HAMSOM is given in Backhaus (1985) and (Pohlmann, 1996).

The main HAMSOM equations are:

$$\begin{aligned}
\frac{\partial u}{\partial t} &= u\frac{\partial u}{\partial x} + v\frac{\partial u}{\partial y} + w\frac{\partial u}{\partial z} + \frac{1}{\rho}\frac{\partial \rho}{\partial x} = fv + A_h\left[\frac{\partial^2 u}{\partial x^2} + \frac{\partial^2 u}{\partial y^2}\right] + \frac{\partial \tau_x}{\partial z} \\
\frac{\partial v}{\partial t} &= u\frac{\partial v}{\partial x} + v\frac{\partial v}{\partial y} + w\frac{\partial v}{\partial z} + \frac{1}{\rho}\frac{\partial \rho}{\partial y} = -fu + A_h\left[\frac{\partial^2 v}{\partial x^2} + \frac{\partial^2 v}{\partial y^2}\right] + \frac{\partial \tau_y}{\partial z}
\end{aligned} \tag{2.1}$$

where u, v and w are the components of the flow field in the eastern, northern and vertical directions, ρ is the water density, f is the Coriolis parameter, A_h is horizontal turbulent viscosity and τ_x and τ_y are components of the wind shear stress. The motion equations 2.1 are completed by the equation of continuity:

$$\frac{\partial u}{\partial x} + \frac{\partial v}{\partial y} + \frac{\partial w}{\partial z} = 0 \tag{2.2}$$

and by the hydrostatic equation:

$$\frac{\partial \rho}{\partial z} = -\rho g \tag{2.3}$$

with g being the gravity acceleration. Vertical eddy viscosity A_{Iv} is parameterized using a method developed by Kochergin (1987). The vertical diffusion coefficients A_{Mv} are calculated by:

$$A_{Mv} = A_{Iv}/S_M \tag{2.4}$$

where S_M is the turbulent Schmidt-Prandtl number.

HAMSOM is based on a semi-implicit formulation of the gravity waves and the vertical mixing. This allows performing simulations for time periods up to a decade with realistic results.

The model has been applied and validated for different shelf regions in the world, such as the North Sea, the Baltic Sean, South China Sea, the Bohai Sea,

the Malacca Strait, the Java Sea, the upwelling zones at the North-west African coast, the Gulf of California, the Canadian waters around Vancouver Island, the Australian west coast, and the Kara and Barents Seas (Backhaus and Hainbucher, 1987; Rodriguez et al., 1991; Stronach et al., 1993; Pohlmann, 1996; Simionato et al., 2001).

2.1.2 SPM transport with ocean currents

SPM concentration in water results from the sum of sources, sinks, and is transported by the flow field. SPM is advected by currents forced by wind stress, horizontal and vertical water density gradients, as well as by the predominant semidiurnal lunar tide M2. Behavior of SPM with the concentration C and with sources C_{source} and sinks C_{sink} is described by:

$$\frac{\partial C}{\partial t} = \frac{\partial}{\partial x}\left(Av_x\frac{\partial C}{\partial x}\right) + \frac{\partial}{\partial y}\left(Av_y\frac{\partial C}{\partial y}\right) + \frac{\partial}{\partial z}\left(Av_z\frac{\partial C}{\partial z}\right)$$
$$-\left(u\frac{\partial C}{\partial x} + v\frac{\partial C}{\partial y} + w\frac{\partial C}{\partial z}\right) + C_{source}\left(t,x,y,z\right) - C_{sink}\left(t,x,y,z\right) \qquad (2.5)$$

Horizontal advection of SPM is calculated using components of the flow field in the eastern and northern directions (u and v). Vertical component of flow field (w) is calculated from u and v using the continuity equation 2.2. Horizontal turbulent diffusion coefficients (Av_x and Av_y) are calculated by the circulation model HAMSOM. The vertical turbulent diffusion coefficient Av_z is calculated as described in Section 2.1.3.

2.1.3 Vertical processes in the water column

Currents velocity gradients and water perturbations at the surface due to wind stress and waves determine turbulence in the North Sea. In the near seabed water layers turbulence occurs due to bottom friction and seawater stratification. Vertical turbulent diffusion and the vertical component of advection distribute SPM in the water column. The vertical diffusion coefficient $Av_z(m^2\ s^{-1})$ includes

two components describing the action of waves and ocean currents.

$$Av_z = Av_{cur} + Av_{wave} \tag{2.6}$$

The contribution of ocean currents Av_{cur} $(m^2\ s^{-1})$ can be obtained from the equation describes the currents speed shear in neighboring layers (Pleskachevsky et al., 2005).

$$\frac{\partial U}{\partial Z} = \frac{Av_{cur}}{Ak_{cur}^2} \tag{2.7}$$

The diffusivity coefficient $Ak_{cur}^2 = U^2/g$ is the Prandl's mixing length with the current velocity $U(m\ s^{-1})$ and gravitational acceleration $g(m\ s^{-2})$. The wave component Av_{wave} $(m^2\ s^{-1})$ represents the kinetic wave energy calculated as a function of significant wave height $Hs(m)$, wave number $k(m^{-1})$, peak period $T(s)$ and the maximum orbital wave velocity $U_w(m\ s^{-1})$.

$$Av_{wave} = (k * Hs)^2 * U_w^2 * T \tag{2.8}$$

The change in SPM concentration due to gravitational sinking $C_{sink}(kg\ m^{-3})$ over the time step Δt is calculated using the actual concentrations of SPM $C(kg\ m^{-3})$ in each model layer with thickness $h(m)$ and a sinking velocity $W_{sink}(m\ s^{-1})$.

$$\frac{\partial C_{sink}}{\partial t} = C\frac{W_{sink}}{h} \tag{2.9}$$

For the entire water column, the SPM concentration in each layer increases due to sinking from the layer above and decreases due to sinking into the layer below.

2.1.4 Exchange processes at the seabed - water interface

Turbulent intensity due to waves and currents in the near-bottom water layer is represented in the model by the shear stress velocity V^* $(m\ s^{-1})$. It drives the processes at the interface between water and seabed, i.e. sedimentation, resuspension and erosion and is calculated from the shear stress τ and actual water density ρ:

$$V^* = \sqrt{\tau/\rho} \tag{2.10}$$

The mean shear stress τ_{mean} $(kg\ s^{-2}\ m^{-1})$ is defined as a two-coefficient pa-

rameterization (Soulsby, 1997) due to current τ_{cur} and wave τ_{wave}:

$$\tau_{mean} = \tau_{cur}\left[1 + 1.2\left(\frac{\tau_{wave}}{\tau_{cur} + \tau_{wave}}\right)^{3.2}\right] \tag{2.11}$$

The maximum of shear stress τ_{max} is needed to determine the threshold of motion with the angle between currents and wave direction ϕ:

$$\tau_{max} = \sqrt{\left(\tau_{mean} + \tau_{wave}\cos\phi\right)^2 + \left(\tau_{wave}\sin\phi\right)^2} \tag{2.12}$$

The currents component of shear stress τ_{cur} is calculated from the quadratic friction law with the currents velocity in the lowest water layer $U\ m\ s^{-1}$ and the friction coefficient C_D:

$$\tau_{cur} = \rho C_D U^2 \tag{2.13}$$

where C_D is defined as:

$$C_D = 0.16\left(1 + \ln\left(\frac{Z_0}{H_{kb}}\right)\right)^{-2} \tag{2.14}$$

where the roughness length in meters $Z_0 = d_{50}/12$ with the mean grain size $d_{50} = 0.00025(m)$ and $H_{kb}(m)$ is the thickness of the lowest water layer.

The waves component of shear stress τ_{wave} $(kg\ s^{-2}\ m^{-1})$ with the maximum of the horizontal orbital wave velocity U_w and the wave friction factor f_w is calculated as:

$$\tau_{wave} = 0.5\rho f_w U_w^2 \tag{2.15}$$

Assuming an equivalent sine wave for the significant wave height H_s, peak period T, and wave number k at a water depth h U_w is calculated as:

$$U_w^2 = \frac{\pi H_s}{T\sinh\left(kh\right)} \tag{2.16}$$

The wave friction factor f_w is determined by the maximum of the rough bed friction f_{wr} and the smooth bed friction f_{ws} coefficients:

$$f_{wr} = 0.237\left(\frac{A}{k_s}\right)^{-0.52}, f_{ws} = BR_w^{-N} \tag{2.17}$$

The parameter $k_s = 2.5d_{50}$ is the Nikuradse roughness length, related to grain size for hydrodynamically rough flows. $A = U_w T/2\pi$ is the semi-orbital excursion. The

parameters of the smooth bed friction factor f_{ws} depend on whether the motion is laminar or turbulent, which can be distinguished with the help of the Reynolds number R_w with the kinetic viscosity $\nu = 0.0000012(m^2\ s^{-1})$:

$$R_w = \frac{U_w A}{\nu} \tag{2.18}$$

Finally, the parameters B and N are defined as follows:

$$\begin{array}{lcll} \text{if } R_w \leq 5 \times 10^5 \textit{ (laminar)} & \Rightarrow & B = 2, & N = 0.5 \\ \text{if } R_w > 5 \times 10^5 \textit{ (turbulent)} & \Rightarrow & B = 0.0521, & N = 0.187 \end{array}$$

The choice of threshold values for V^* is based on the analysis of measured and experimental data for the German Bight (located in the south-eastern part of the North Sea) and the North Sea described in Pohlmann and Puls (1994); Gayer et al. (2006)). In this study, the follow values are used:

$$\begin{array}{lccccl} \text{sedimentation} & V^* & < & V^*_{sed} & = & 0.0099\ m\ s^{-1} \\ \text{resuspension} & V^* & > & V^*_{res} & = & 0.0100\ m\ s^{-1} \\ \text{erosion} & V^* & > & V^*_{ero} & = & 0.0280\ m\ s^{-1} \end{array}$$

Sedimentation starts when conditions in the near-bottom water layer are calm and V^* drops below the threshold value V^*_{sed} . Sedimentation decreases the SPM content in the lowest water layer and increases the SPM mass in the upper seabed layer. The change of SPM mass per unit area $M_{sed}(kg\ m^{-2})$ over the time $\Delta t(s)$ is calculated as:

$$\frac{\partial M_{sed}}{\partial t} = C_b * W_{sink} \left(1 - (V^*/V^*_{sed})^2\right) \tag{2.19}$$

with $C_b(kg\ m^{-3})$ being the actual SPM concentration in the bottom water layer.

Resuspension occurs when V^* reaches the threshold value V^*_{res} . Then, the total mass content of the upper seabed layer is resuspended into the bottom water layer.

Erosion starts when V^* exceeds the threshold value V^*_{ero} . The SPM mass is completely removed from the seabed layers down to the depth of erosion $h_{ero}(m)$.

$$h_{ero} = k_{ero} * (V^{*2} - V^{*2}_{ero})/V^{*2}_{ero} \tag{2.20}$$

Experimental coefficient $k_{ero} = 0.001m$ is adjusted to represent conditions typical for the North Sea (Pleskachevsky et al., 2005).

2.1.5 Seabed processes

The model considers the upper 20 cm of the seabed. Exchange between bed layers due to biotic activity is modeled by a diffusion equation with a coefficient for bioturbation $Av_{bio}(m^2\ s^{-1})$

$$\frac{\partial M}{\partial t} = \frac{\partial}{\partial z}\left(Av_{bio}\frac{\partial M}{\partial z}\right) \tag{2.21}$$

To simulate the effect of bioturbation, the value of Av_{bio} is calculated for each model grid point depending on the season s_f, location l_f, and depth in the bottom h_f.

$$Av_{bio} = Av_{bio}^{max} * s_f * l_f * h_f \tag{2.22}$$

Diffusion coefficient for bioturbation Av_{bio}(Eq. 2.22) decreases from 100 $cm^2\ a^{-1}$ at the seabed surface to 20 $cm^2\ a^{-1}$ at 20 cm depth. Av_{bio}^{max} represents the highest possible bioactivity. It decreases linearly (Pohlmann and Puls, 1994) with depth in the seabed indicating that more bioactivity occurs in the upper seabed levels. The seasonal factor s_f depends on the month with a seasonal maximum of bioactivity in October ($s_f = 0.99$) and minimum in April ($s_f = 0.54$) (Fig. 2.1c). Intensity of bioactivity in different regions of the model area is described by two factors:
(a) The factor l_f (range 0.6 - 1) (Fig. 2.1a) depends on content of fine sediment in the seabed and
(b) The factor h_f ranges from 0.2 to 1 (Fig. 2.1b). It depends on the depth in the North Sea.
The product s_f*l_f*h_f varies from 0.07 to 0.99. All factors are empirical and based on Puls (2006) and model test studies.

2.2 Model setup and forcing

Diagram of the model concept (Fig. 2.2) shows the data flow for the SPM modeling. Model simulation covers the time period of two years starting in the beginning of 2002 until the end of 2003. The year 2002 was then used for the detailed analysis of model results with regard to instant processes governing the dynamics of SPM and to compare model results with available in-situ and satellite measurements.

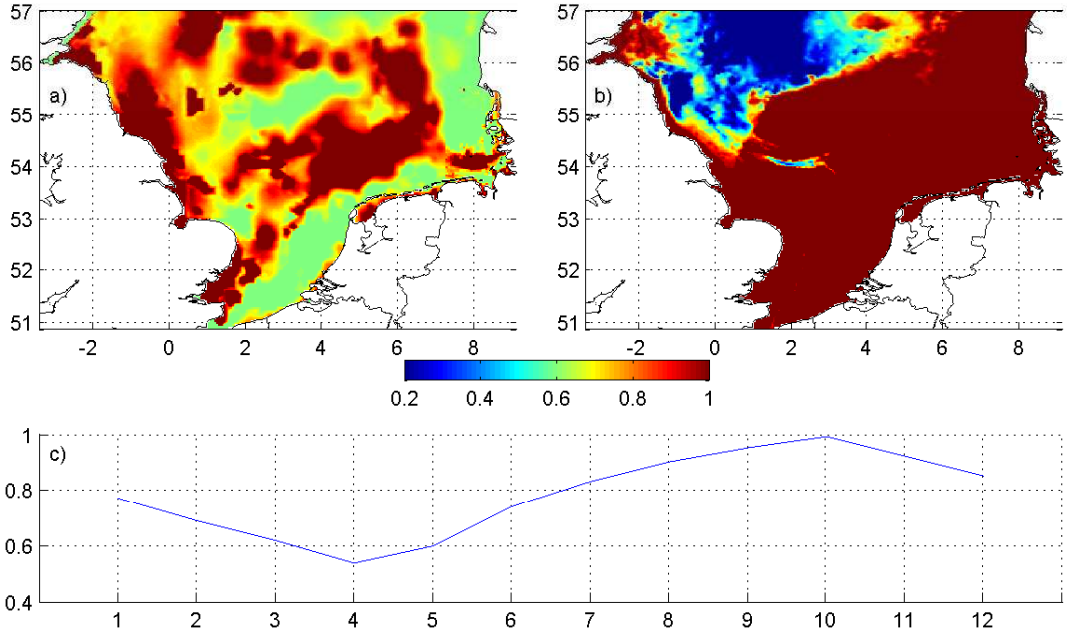

Figure 2.1: Bioturbation parameters: a) fine sediment content factor (l_f), b) depth factor (h_f) and c) seasonal factor (s_f).

However, satellite data assimilation was performed only for the year 2003 when data became available for the full year.

Initial concentration field of SPM in water, initial content of fine sediment in the seabed, as well as the boundary conditions, meteorological and waves forcing will be described in details in this section.

2.2.1 Model region

The region of interest is the southern part of the North Sea from $50.87°N$ to $57.17°N$ and from $3.40°W$ to $9.10°E$. It is a shallow region with an average depth of about 55 m (Fig. 2.3). The model grid has a horizontal resolution of 1.5' in the north-south direction and 2.5' in the east-west direction (corresponding to about 2.5-3 km). The model has 21 vertical layers in water and 21 layers in seabed. The model layers depth in water is variable from 5 m in the upper layers up to 10 m in the lower layers. The layers thickness in the seabed increases from 0.5 mm in the upper layers to 5 cm in the lower layers.

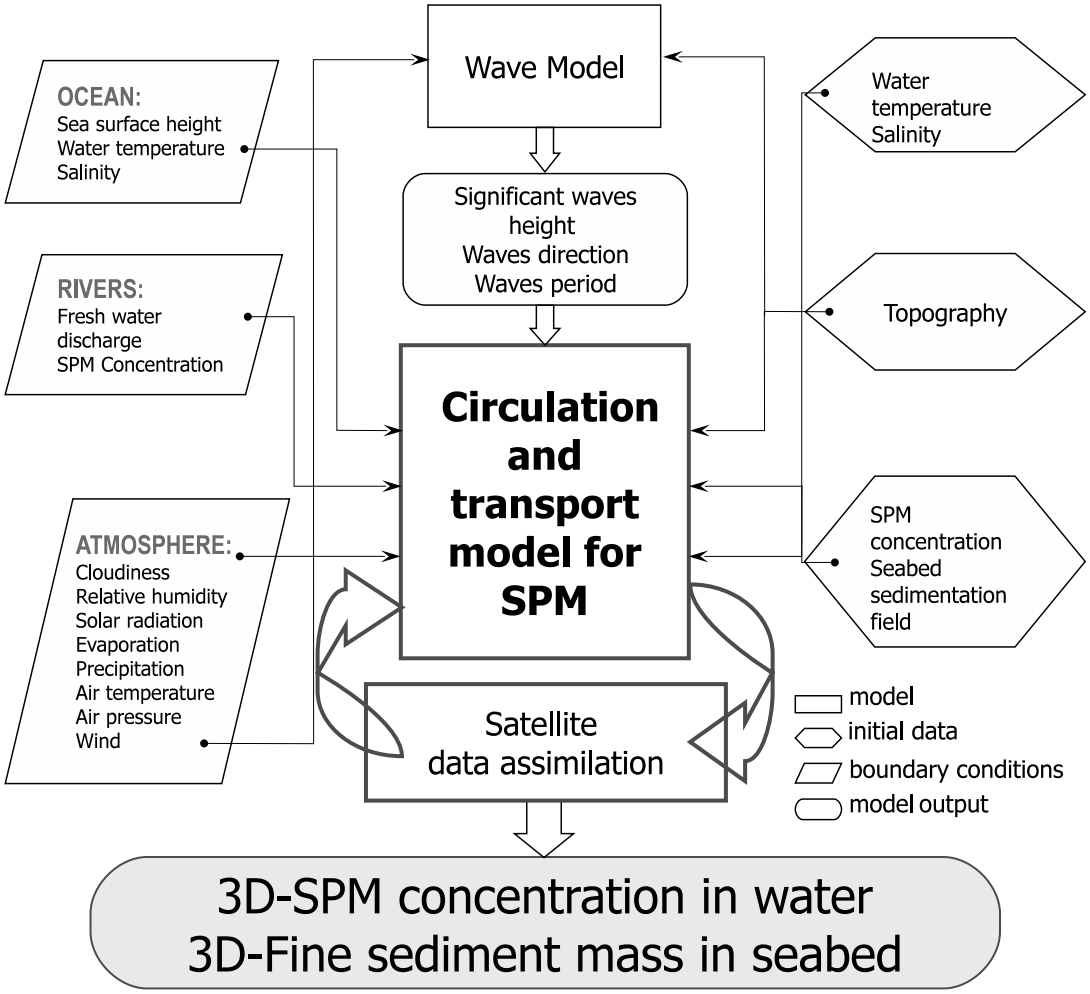

Figure 2.2: Model concept and data flow.

2.2.2 SPM fractions in the model

The SPM concentration in the model is represented by three fractions (SPM1, SPM2 and SPM3) with different particle size (K_{size}) and sinking velocity (W_{sink}) (see Table 2.1). The three SPM fractions, ranging in grain size from $< 20\mu m$ to $63\mu m$ are chosen so that they correspond to representative sizes of measured SPM in the North Sea (Eisma and Kalf, 1987). SPM 1 and SPM 2 fractions represent two different types of fine sediment in water with the grain size $< 20\mu m$ and different sinking velocity. SPM3 represents the larger SPM fraction with the grain size $63\mu m$. The sinking velocities of fractions SPM1 and SPM2 are based on the measurements in the German Bight in January-February 1993 (Puls

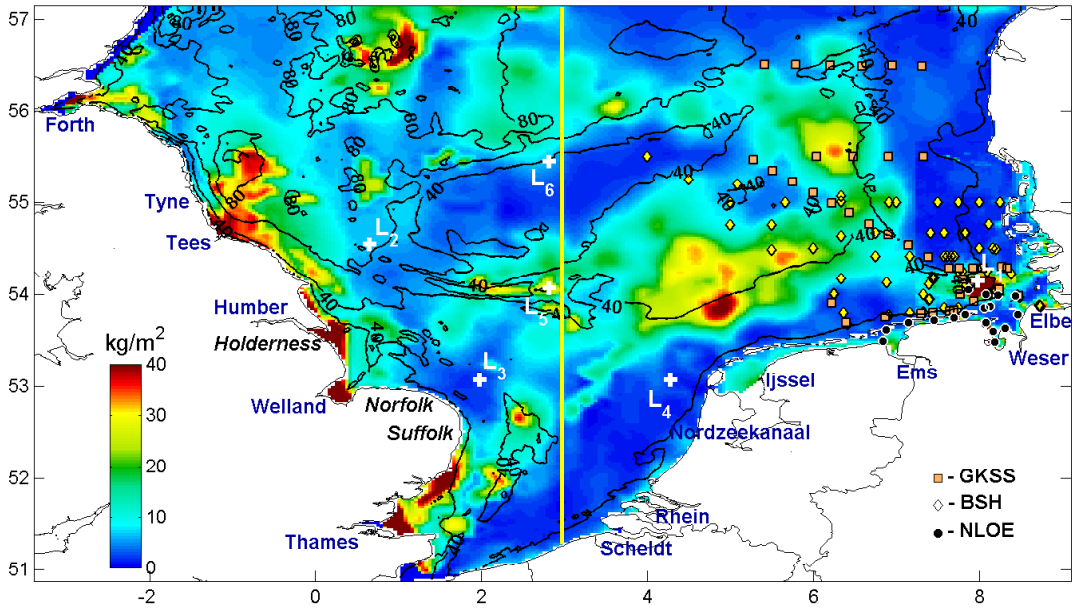

Figure 2.3: Model area, initial seabed distribution of fine sediment ($< 20\mu m$) fraction (colors in $kg\ m^{-2}$) and bathymetry (lines, depth in m) on a grid of 1.5' by 2.5'. Geographical locations of points selected for time series analysis (L1, L2, L3, L4, L5 and L6), as well as points where measured SPM concentrations in water (color markers) were available for model evaluation are indicated. English cliffs (black labels) and rivers (blue labels) are shown. A line along 3° E shows vertical section referred to Fig. 5.6.

et al., 1995). The sinking velocity of SPM3 fraction is calculated using the Stokes formula for silt grain with a size of $40\mu m$. SPM concentration in water, rivers, near cliffs and open model boundaries is formed as a sum of these three fractions in different proportions (Table 2.1).

2.2.3 Initial SPM concentration in water

Model calculations in water were initialized with the vertically integrated SPM concentrations that reproduce the typical SPM distribution in the North Sea for each SPM fraction depending on the depth in each grid point (Table 2.1). The vertical profile of SPM concentration in the water column in the beginning of the simulation (the first few days), as well as the resuspension layer on the seabed are formed mainly by sinking of SPM. The initial SPM concentration forms the

Table 2.1: Summary of SPM fractions. SPM particle size, sinking velocity and percentage distribution in the sources and initial seabed field.

Fractions		SPM 1	SPM 2	SPM 3
Particle size, $K_{size}[\mu m]$		< 20	< 20	20-63
Sinking velocity, $W_{sink}[mm\ s^{-1}]$		0.10	0.02	1.00
Content [%]	North Atlantic	88.0	12.0	0.0
	English Channel	12.5	87.5	0.0
	English Cliffs	40.0	20.0	40.0
	Rivers, f_{riv}	25.0	50.0	25.0
	Seabed, f	80.0	20.0	-
Initial range in water (upper-lowers layers) $[mg\ l^{-1}]$		0.5-5.0	0.1-1.0	0.05-0.5

background distribution of SPM in water. This assumption allows to capture the zones with high and low SPM contents in the North Sea in order to achieve more realistic SPM distributions before the first strong mixing event with resuspension and erosion. After the mixing event occurs, all processes are fully involved in the modeling.

2.2.4 Initial fine sediment content in the seabed

The seabed distributions of fine sediment fractions SPM1 and SPM2 are used to calculate the initial content of fine sediment in the seabed (Fig. 2.3). Initially, the fine sediment map was generated from the measured grain size data (Gayer et al., 2004). In the German Bight and in the eastern part of the North Sea, the map was improved using surface SPM concentrations retrieved from satellite data MOS (Modular Optoelectronic Scanner) and eroded SPM mass calculated by an SPM model (Pleskachevsky et al., 2005). The MOS scene on 03.02.2000 captured a storm in the North Sea coming from the North Atlantic (28.01.2000-04.02.2000). According to the maximal wave height, the storm peak occurred on 30.01.2000. Surface SPM concentrations calculated from the MOS scene after the storm peak were therefore smaller than the highest SPM concentrations possible under the waves with the heights of about 10 to 12 m. In order to compensate this deficiency, an SPM model (Pleskachevsky et al., 2005) calculated the relative change of SPM concentration in the upper water model layer between the storm peak and the MOS scene. Model results showed that the average decrease of SPM

mass after the storm peak was about 10% in the whole model domain (mainly due to sinking). This difference was added to MOS data in every grid point resulting in the SPM concentration during the storm peak determined backwards in time.

The contribution of erosion into the SPM concentration during the storm was determined by subtracting the SPM concentration typical for the calm weather conditions in the North Sea (Doerffer and Fischer, 1994) from the SPM concentration calculated for the storm peak. Eroded SPM mass in seawater per unit area was estimated as the product of SPM concentration and depth assuming that under strong storm conditions SPM in shallow water areas (up to 40 m) is totally mixed and homogeneously distributed in the water column.

The seabed sediment map was corrected to attain the eroded SPM mass in water according to erosion depth (h_{ero}), obtained as the function of bottom shear stress velocity (see Eq. 2.20). For more details about the method used for the processing of fine sediment map, see Pleskachevsky et al. (2002, 2005) and Gayer et al. (2006).

The three-dimensional initial sediment mass M ($kg\ m^{-2}$) of each sediment fraction in the seabed layer with the depth z_b (m) for the fractions SPM1 and SPM2 ($f_{1,2}$; Table 2.1) is calculated using:

$$M_{1,2} = f_{fine} * f_{1,2} * z_b * \rho_{dry} \tag{2.23}$$

For the fraction SPM3 it is:

$$M_3 = 39 * \sin\left(f_{fine}/32\right) * z_b * \rho_{dry} \tag{2.24}$$

The dry density of fine sediment in this study is $\rho_{dry} = 1300\ kg\ m^{-3}$.

2.2.5 SPM concentrations in the rivers, cliffs and open boundaries

The seabed is the main source of SPM in North Sea and predominantly determines the SPM distribution in the water. Additional sources of SPM in the model are rivers, English cliffs (Fig. 2.4) and the open boundaries. The hourly fresh

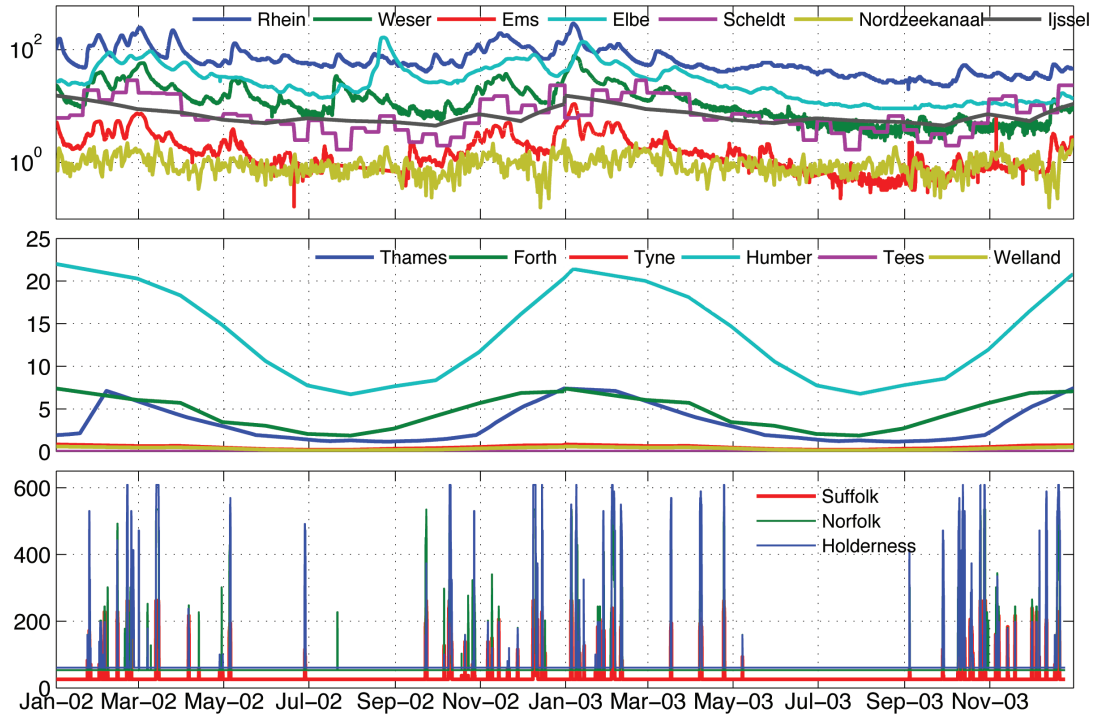

Figure 2.4: Loads of SPM ($kg\ s^{-1}$) to the North Sea in the continental (a), UK rivers (b) and English cliffs (c) in 2002 and 2003. Geographical locations are shown on the map (Fig. 2.3).

water discharges from the rivers Elbe, Weser, Ems and Rhine (DOD, 2006), the daily fresh water discharges from Ijssel, Nordzeekanaal and Scheldt (Pätsch and Lenhart, 2004), as well as climate monthly discharges from the rivers Thames, Welland, Humber, Tees, Tyne and Forth (GRDC, 2006) are linearly interpolated to fit the temporal resolution of the model. The rivers load of SPM L_{riv} ($kg\ s^{-1}$; Fig. 2.4a, b) is calculated as the product of the fresh water discharge D_{riv} ($m^3\ s^{-1}$) and the annual mean SPM concentration (Gayer et al., 2004) in each river C_{riv} ($kg\ m^{-3}$).

$$L_{riv} = D_{riv} * C_{riv}. \tag{2.25}$$

The concentration change of SPM for each fraction due to rivers C_{riv} ($kg\ m^{-3}$) is calculated using the actual water volume Vol (m^3) in the grid cells where the rivers enter the model domain and contents of the three SPM fractions in the

rivers load (f_{riv}; Table 2.1):

$$\frac{\partial C_{riv}}{\partial t} = f_{riv}\frac{L_{riv}}{Vol} \tag{2.26}$$

Note that in 2003, the fresh water discharge and SPM loads were reduced in the major rivers (i.e. Rhine, Elbe and Weser) up to one order of magnitude compared to 2002 because of the extremely high temperatures and low precipitation rate in the central and western parts of Europe.

The contribution of the English cliffs into the SPM concentration (Fig. 2.4c) is based on long-term measurements of annual mean amounts of eroded SPM from Suffolk (50 $kg\ s^{-1}$), Norfolk (45 $kg\ s^{-1}$) and Holderness (58 $kg\ s^{-1}$). The SPM loads from cliffs depend stepwise on whether storm or calm conditions occur (Fig. 2.4c). Storm conditions in the model start when significant wave heights near the coast are $> 2\ m$, based on the three years wave-height statistics near cliffs (Gayer et al., 2006). The modeled by the WAM model significant wave height field for the year 2002 and 2003 was used to calculate SPM load from cliffs.

Open boundary conditions are the sea surface elevation induced mainly by tides (obtained from the large-scale HAMSOM model domain for the North Atlantic) and climatic averages of temperature and salinity (based on the NCEP re-analysis).

SPM concentration at the open boundaries of the North Atlantic and the English Channel is constant in time and vertically integrated over the water column with values of 5 and 8 $mg\ l^{-1}$ respectively (Gayer et al., 2006; Puls et al., 1997). The distribution between the SPM fractions in the English cliffs and at the open boundaries is given in Table 2.1.

2.2.6 Meteorological data

Meteorological forcing including the wind components, atmospheric pressure, air temperature, relative humidity and cloudiness is based on hourly data calculated by the Regional Model of atmosphere REMO (Feser et al., 2001). The REMO model based on the primitive equations in a terrain-following hybrid coordinates system. The model has a resolution of 0.5° and model area from 19.5°W to

$20.5°E$ and from $25.0°S$ to $20.0°N$. REMO is forced with NCEP (National Centers for Environmental Prediction) reanalysis (National Centers for Environmental Prediction, 2005).

2.2.7 Wave data

Wave forcing is calculated by the spectral ocean wave model WAM (Wave Analysis Model; WAMDI Group (1988); Günther et al. (1992); Komen et al. (1994)). A third-generation wave model WAM calculates the wave spectrum $F(f, \theta, \phi, \lambda)$ where the arguments are frequency f, direction θ, latitude ϕ and longitude λ.

$$\frac{dF}{dt} + \frac{\partial}{\partial\phi}\left(\dot{\phi}F\right) + \frac{\partial}{\partial\lambda}\left(\dot{\lambda}F\right) + \frac{\partial}{\partial\theta}\left(\dot{\theta}F\right) = S \tag{2.27}$$

The source function S represents the physical mechanisms that are involved in the evolution of the wave field (WAMDI Group, 1988) as a superposition of the wind input S_{in}, white capping dissipation S_{dis} and nonlinear transfer S_{nl}

$$S = S_{in} + S_{dis} + S_{nl} \tag{2.28}$$

The parameterization of the spectral shape and source function S are solved implicitly by solving the equation of energy transport in the prognostic part of the spectrum with the wave group velocity C_g.

The WAM model on a Cartesian grid in this study was first applied for the North Atlantic on a coarse grid forced by the wind field from the NCEP reanalysis. Then it was applied for the southern North Sea with the depth-induced refraction option (on the same grid as the CTM-SPM model, nested in the coarse grid) forced by wind from the REMO data and using the boundary conditions from the WAM run for the North Atlantic. Significant wave heights, wave periods (TM1) and wave directions represent the wave forcing in the CTM-SPM model.

Chapter 3

Assimilation of satellite data into the model: method description and setup

Ocean color measurements comprise a significant amount of available satellite data. Ocean color is determined by suspended and dissolved substances present in seawater. It is determined by the interactions of incident light with substances or particles present in the water. The most significant constituents are freely floating photosynthetic organisms (phytoplankton) and inorganic particulates. Phytoplankton contains chlorophyll, which absorbs light at blue and red wavelengths and transmits light in the green part of the spectrum. Particulate matter can reflect and absorb light reducing transparency and light transmission of the water. The term "ocean color data" refers to the accurate measurements of light intensity at visible wavelengths. The scattering of non-absorbing particles can be related to the total suspended matter (TSM) concentration. Phytoplankton pigment absorption is related to chlorophyll α concentration, which can be used as an indicator of organic component of total suspended matter (OSM). The difference between TSM and OSM represents the inorganic suspended matter (ISM).

This chapter describes how satellite data is used in SPM simulations: Method of satellite data assimilation is given in Section 3.1. Section 3.2 shows how satellite data is processed in order to produce concentrations of SPM from the optical view images. To remove unrealistic values from satellite data, quality control system

was developed in this study (Section 3.3). Satellite data assimilation setup is described in Section 3.4.

3.1 Method of data assimilation: optimum interpolation

Optimum interpolation (OI; Lionello and Günther (1992)) is used to construct analyzed surface SPM concentration (C_A^i) field. The C_A^i at each grid point is produced using a linear combination of the first-guess concentration field calculated by the model C_P^i, and the observed concentration field C_O^i:

$$C_A^i = C_P^i + \sigma_P^i \sum_{j=1}^{N_{obs}} W_{ij} \frac{C_O^j - C_P^j}{\sigma_P^j} \tag{3.1}$$

with N_{obs} being the number of available observations. σ_P^i is the root-mean-square error in the model prediction,

$$\sigma_P^i = \left\langle \left(C_P^j - C_T^j \right)^2 \right\rangle^{1/2} \tag{3.2}$$

C_T^j represents the true value of C. The weights W_{ij} are chosen to minimize the root-mean-square error in the analysis, σ_A^j,

$$\sigma_A^i = \left\langle \left(C_A^j - C_T^j \right)^2 \right\rangle^{1/2} \tag{3.3}$$

Assuming that the errors in the model are uncorrelated with the errors in the measurements, the solution is

$$W_{ij} = \sum_{k=1}^{N_{obs}} P_{ik} M_{kj}^{-1} \tag{3.4}$$

where the element of the matrix M is

$$M_{kj} = P_{kj} + O_{kj} \tag{3.5}$$

and P and O are the error correlation matrices of prediction and observation, respectively scaled with σ_P^i:

$$P_{kj} = \left\langle \frac{\left(C_P^k - C_T^k\right)\left(C_P^j - C_T^j\right)}{\sigma_P^k \sigma_P^i} \right\rangle \tag{3.6}$$

$$O_{kj} = \left\langle \frac{\left(C_O^k - C_T^k\right)\left(C_O^j - C_T^j\right)}{\sigma_P^k \sigma_P^j} \right\rangle \tag{3.7}$$

Therefore the prediction error correlation matrix P and the observation error correlation matrix O must be specified. This would require the determination of statistics for both prediction and the observations, which are presently unavailable. For the prediction it is assumed

$$P_{kj} = exp\left(-\frac{|\bar{x_k} - \bar{x_j}|}{L_{max}}\right) \tag{3.8}$$

where L_{max} is the radius of influence. The observation O_{ij} errors are assumed to be random and uncorrelated:

$$O_{ij} = \delta_{ij}\left(\sigma_O^i / \sigma_P^i\right) = \delta_{ij} R_i \tag{3.9}$$

Definition of the assimilation method parameters used in this study is given in section 6.1.

3.2 Satellite data processing

MERIS (medium-spectral resolution, imaging spectrometer) is designed to acquire 15 spectral bands in the 390 - 1040 Nm range of the electromagnetic spectrum. MERIS data are provided at 3 different levels of processing (Level 0, Level 1, Level 2) and at 3 different spatial resolutions (full, reduced and low). For the same image, a full-resolution (FR) image has 4x4 more points (pixels) than the same image in reduced-resolution (RR), and an RR image has 4x4 more points (pixels) than the same image in low-resolution (LR). Accordingly, a pixel in an FR image represents an area of 260 m x 290 m, in an RR image an area of 1,040 m x 1,160 m and in LR an area of 4,160 m x 4,640 m.

More than 400 scenes (level 1 RR MERIS) selected from the MERIS data for years 2002 and 2003 covering the southern North Sea (see Fig. 2.3) were processed using the C2R (MERIS Case-2 Regional Processor; Doerfer et al. (2006)) to calculate SPM concentrations at the sea surface (Fig. 3.1). In contrast to the year 2002, in which MERIS data was used for the model evaluation purposes, data for the whole year 2003 was used for assimilation.

Satellite data provides suspended matter concentration integrated over the signal (light) penetration depth. It does not give information about the vertical suspended matter distribution within this depth. Generally, satellites underestimate suspended matter concentrations due to algorithmic constraints (Fettweis et al., 2007).

TSM and chlorophyll concentration Chl were used to calculate the inorganic suspended matter ISM concentration, which can be assimilated into the SPM model. Based on the relationships between chlorophyll concentration and biological activity and biomass, the concentration of ISM can be estimated by:

$$ISM = TSM - OSM(Chl) \tag{3.10}$$

where TSM is the total suspended matter and OSM is the organic suspended matter as a function of chlorophyll concentration Chl. OSM concentration can be estimated as the product of the empirical coefficient k and chlorophyll concentration Chl:

$$OSM = k * Chl \tag{3.11}$$

The value of k in this study was set to 4, based on the comparison between measurements of OSM and chlorophyll concentration available from literature (Steele and Baird, 1963; Menzel and Ryther, 1963).

Concentrations of ISM calculated from satellite data according to equation 3.10 are used for comparison with modeled SPM concentrations.

Satellite data are episodic and were collected generally between March and December. From all scenes the average coverage of the southern North Sea is 22.5%, for standard MERIS level 2, 19.2% for MERIS C2R with flags and 17.9% for MERIS C2R with flags and max SPM filter (Fig. 3.2). This data-set can not

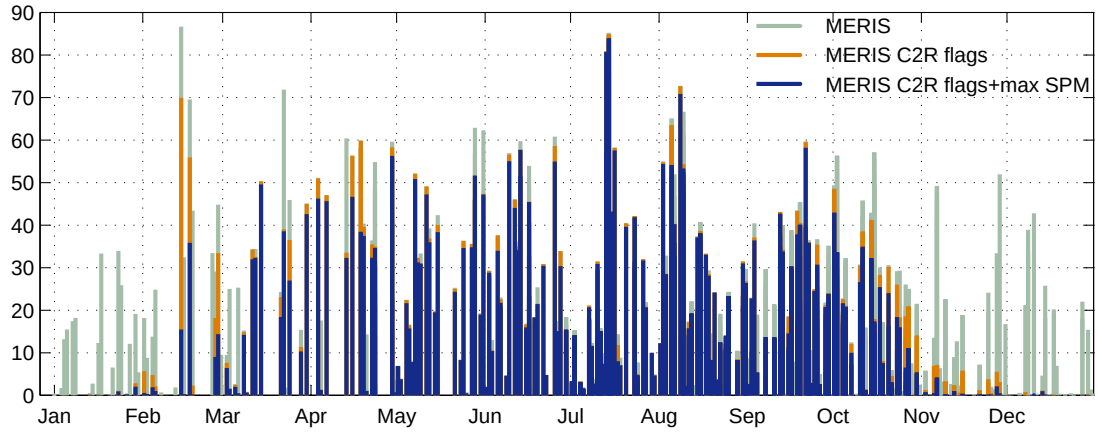

Figure 3.1: Spatial coverage of the southern part of the North Sea (Fig. 2.3) by MERIS data in the year 2003 calculated in % of the model domain.

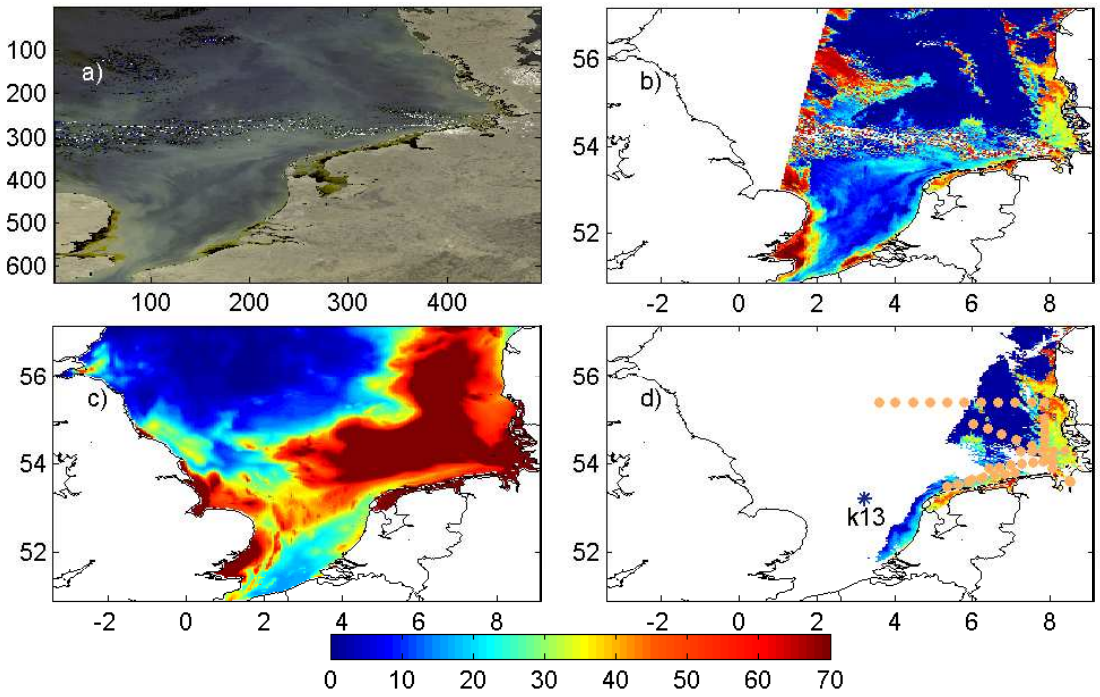

Figure 3.2: MERIS scene on 15.10.2003 at 10:05:36: an RGB view (a), surface SPM concentration ($mg\ l^{-1}$) from level 2 standard processor (b), maximum of modeled surface SPM concentration ($mg\ l^{-1}$) in 2002 (c) and surface SPM concentration ($mg\ l^{-1}$) from level 2 C2R (d, flags on) and location of k13 and in-situ observation points (GKSS cruise 23.04.2003 - 01.05.2003).

be assimilated directly into the model. Figure 3.2b shows the output result of standard MERIS level 2 processing. The SPM concentration patterns located in

the open North Sea can be interpreted only as noise (for example due to clouds or seabed reflection) and must be filtered out.

3.3 Quality control of satellite data

In order to filter out unrealistic values of the surface SPM concentrations obtained from satellite, flags technique was used. It is based on the assumption that the different objects (land or water) on the Earth surface, as well as the atmosphere can have a threshold values of radiance reflectance in different wave lengths. The threshold values drive the flags by comparison with the measurements. The values of flags were set by processing the MERIS level 1 data to level 2.

Three flags (see Table 3.1) available in C2R level 2 product are used for quality control of the MERIS data. Such approach allows removing zones with incorrect concentration (e.g. at cloud rims in the open North Sea; Fig. 3.1 and 3.2b, d). However, the C2R processor is not capable to interpret zones, which are visible in RGB and have plausible SPM structures (Fig. 3.2a) and thus filters them out. In addition to flags filtering, threshold values (C_{max}) for surface SPM concentration in the North Sea based on the model simulation for the year 2002 was used. C_{max} was calculated from hourly mean values as the maximum of modeled surface SPM concentration in every grid point (Fig. 3.2c). MERIS data were corrected using the assumption that the surface SPM concentration obtained from satellite can not be more than C_{max} (Fig. 3.2c).

3.4 Satellite data assimilation setup

The MERIS data were assimilated into the upper model layer in the model time steps, which corresponded to the MERIS time with a time window of 5 minutes (model time step). For the time steps where several MERIS scenes were available the average surface SPM concentration was calculated before assimilation.

The surface SPM concentration in the model is an integral part of the SPM distribution in the entire water column, formed mostly by sinking and vertical

mixing. Therefore, any change of SPM surface concentration must change the whole vertical profile of SPM. The new vertical profile is computed with the assumption that the form of first guess profile is correct. The change of SPM mass in water related to unit area is calculated as the product of depth and the difference of SPM concentration before and after data assimilation. The computed difference of SPM mass in water is added or subtracted in the seabed in order to preserve the total fine sediment mass balance in the whole seabed-seawater system. Such approach is based on the assumption that the surface SPM distribution is mainly (excluding the erosion of English Cliffs located along the British coastline between approximately $52°30'N$ and $53°30'N$) the result of the exchange processes at the seawater-seabed interface and the vertical mixing in water. Moreover, the change of SPM mass in water due to assimilation leads to changes in the seabed not only immediately at an assimilation moment, but also during the next time steps due to vertical processes in the model, such as sinking and deposition.

Table 3.1: Flags of MERIS Case 2 Regional Processor (Doerfer et al., 2006).

Flag	Description
rad-err	This flag is switched on under hazy conditions, when the aerosol optical thickness exceeds a certain degree for which the neural network has not been trained. It is simply checked by the TOA (top of the atmosphere reflectance) radiance reflectance in MERIS band 1. Under these hazy conditions, the separation between reflectance caused by the atmosphere or by turbid water can fail.
l2-land	Although the land is flagged already by the level 1 land flag and the coastline flag, conditions occur like dry fallen tidal flats, which are not included in the L1 flag. With the l2-land flag we test if the radiance reflectance in MERIS band 13 (865 nm) is above a threshold value (in this study 0.2). In addition, the rim of clouds maybe flagged.
cloud-ice	This flag indicates very high radiance reflectance indicating clouds, ice or snow. Normally it should not appear, because these pixels should have been excluded from water processing by the level 1 bright flag. Algorithm works as for l2-land, the threshold value is 0.07.

Chapter 4

Dynamics of forcing factors

Currents and waves are two equally important factors that force the SPM dynamics in the North. They influence the turbulence intensity and vertical mixing in the water column, as well as the shear stress in the near-seabed water layer, which drives the seabed-water SPM exchange processes (Section 2.1.4). This chapter describes the dynamics of currents (Section 4.1), waves (Section 4.2) and shear stress velocity (Section 4.3) averaged over the *calm* (15 April - 15 October) and *storm* (15 October - 15 April) periods. Such mean seasonal values of significant wave height and the maximum seasonal currents velocity can be used to detect areas in the North Sea with potentially high shear stress velocity that are prone to frequent erosion and resuspension processes.

4.1 Currents

The general circulation patterns with the counter-clockwise direction of currents in the North Sea (Lenhart and Pohlmann, 1997) are mainly formed due to the Atlantic and English Channel inflow during the predominant lunar M2-tide cycles (Bartels, 1957). The tidal component of the currents prevails over the whole currents system. Therefore the currents velocity distribution in the North Sea does not differ significantly during calm and storm periods (Fig. 4.1) as well as between the years 2002 and 2003.

This phenomenon leads to the permanently strong influence of currents on the

shear stress velocity in the shallow regions such as the German Bight, along the British coast and in the English Channel. As shown in the following section (see Section 4.3, Fig 4.3c and d) the currents component of the shear stress velocity alone is sufficiently high for the resuspension during both the calm and the storm periods. However, due to higher wind velocities during the storm period, the maximum of surface currents velocity increases from 0.6 $m\ s^{-1}$ to 1 $m\ s^{-1}$ in the shallow region.

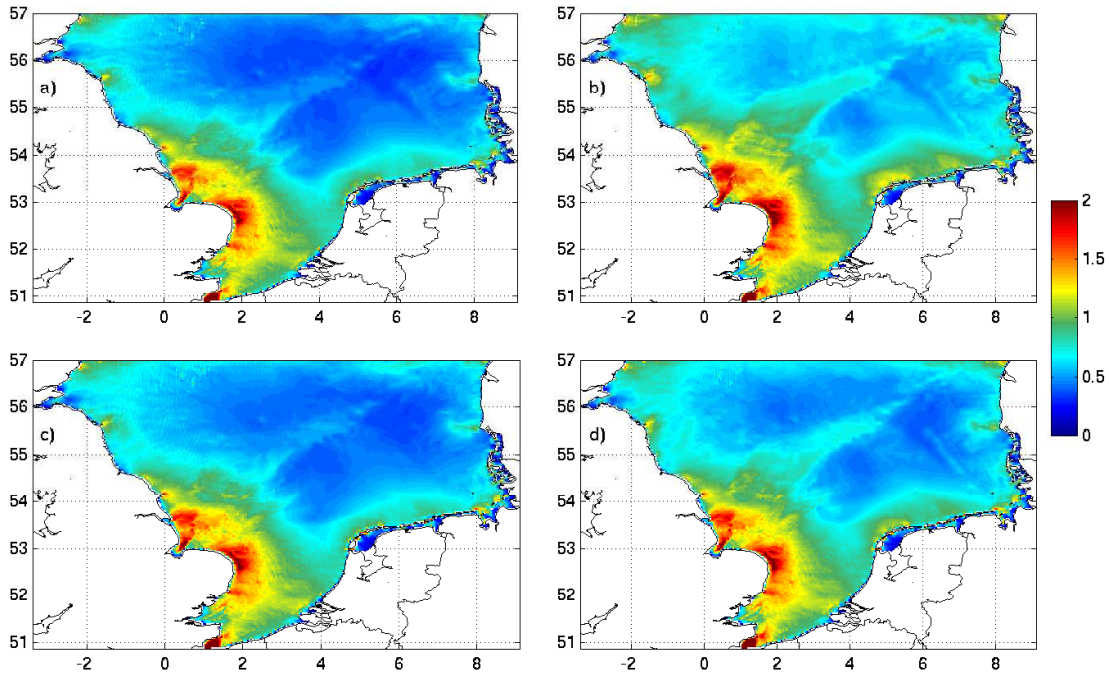

Figure 4.1: Seasonal maximum of surface current velocity ($m\ s^{-1}$) calculated by the model: a) and c) for the calm (15 April - 15 October) and b) and d) for the storm (15 October - 15 April) seasons for the year 2002 and 2003.

4.2 Waves

In contrast to the currents, strong seasonality in the significant wave height Hs is observed in the North Sea in 2002 and 2003 (Fig. 4.2). The values of Hs can be up to 1.5 m higher during the calm period. The maximum of the seasonally averaged Hs during the calm period in the year 2002 is 1.29 m and 1.03 m in

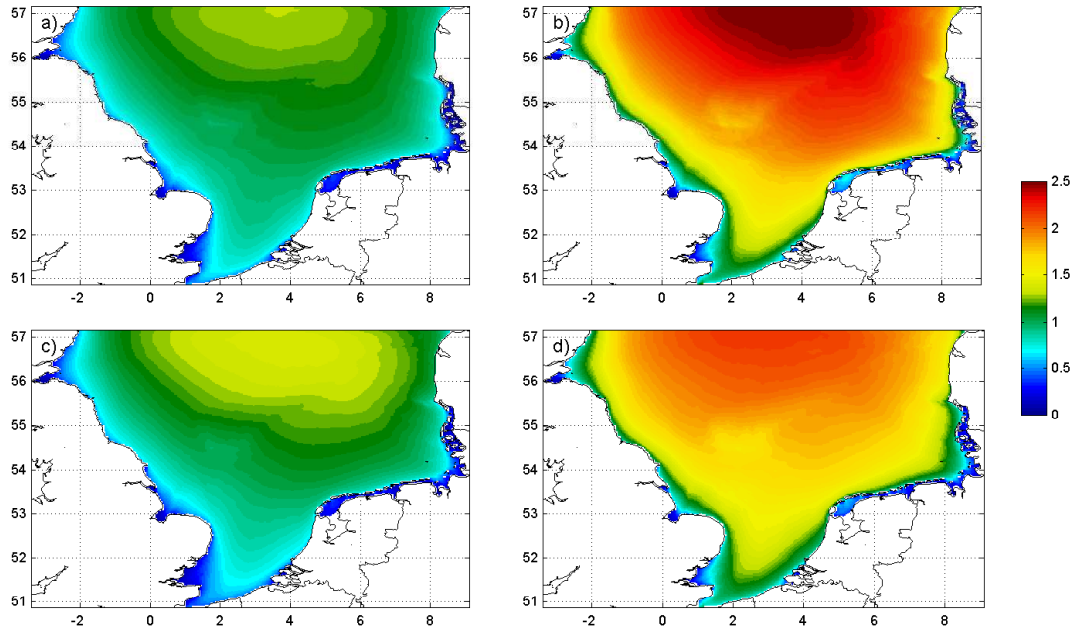

Figure 4.2: Seasonal mean significant wave height (m) calculated by the WAM model: a) and c) for the calm (15 April - 15 October) and b) and d) for the storm (15 October - 15 April) seasons for the year 2002 and 2003.

2003 (Fig. 4.2a and c). During storm period the maximum of seasonally averaged Hs is 2.54 m in 2002 and 2.21 m in the year 2003 (Fig. 4.2b and d).

Although the maximum of the seasonally averaged Hs (2.54 m) is obtained during storm period in the year 2002, the mean of the seasonally averaged Hs during calm period occurred in the year 2003 (1.03 m) exceeds its mean in the year 2002 (0.99 m). It makes potentially more intensive the resuspension process during calm period and can lead to higher surface SPM concentration during calm period in the year 2003. The mean Hs during storm period in 2002 (1.86 m) exceeds its mean in the year 2003 (1.64 m), but more higher mean Hs during calm period in 2002 keeps more SPM in suspension in water column and leads to higher surface SPM concentration in 2003 during storm period, even with smaller maximum of seasonally averaged Hs.

The maximum of Hs is located in the open North Sea throughout both periods because of the topography characteristics, predominant wind direction and storms coming from the North Atlantic. The influence of storm events during the storm

period can be illustrated by the position of the $1.5m$ isoline of the Hs, which is located in the open North Sea during the calm period, and very close to the coast during the storm period.

In the shallow regions, such as the Dogger Bank, the topography effect on the Hs is observed even during the calm period (Fig. 4.2a and b) It is more intensive during the storm period (Fig. 4.2c and d) because of the increase in the Hs values. With regard to the SPM exchange processes at the water-seabed interface, the role of the wave component of the shear stress velocity is significant in the shallow regions during both the calm and the storm periods, where high surface SPM concentrations can be observed, depending on the current weather condition.

4.3 Shear stress velocity

Because of the higher maximal significant wave height in the year 2002 in comparison to the year 2003 during the storm period (Fig. 4.2), the modeled currents and waves for the year 2002 were selected in order to show the maximum of wave influence on the near seabed shear stress in the period of model simulation.

The seasonal mean near seabed shear stress velocity in the year 2002 (V^* , $cm\ s^{-1}$) distribution (Fig. 4.3a and b) allows to classify the southern North Sea in terms of seabed-water exchange processes, indicating different zones with a dominance of one or another process.

In line with the general circulation, the currents component of V^* (Fig. 4.3 c and d) does not differ significantly during the calm and the storm periods. It shows the permanent resuspension zones in the south-eastern part of the North Sea, along the Netherlands coast and in the German Bight. Such pattern explains the high surface SPM concentrations in these areas even under calm condition throughout the whole year.

In contrast to the currents, the effect of waves on the SPM distribution is irregular. But it plays the dominant role during storm periods, when the distribution of V^* changes due to the influence from the wave component.

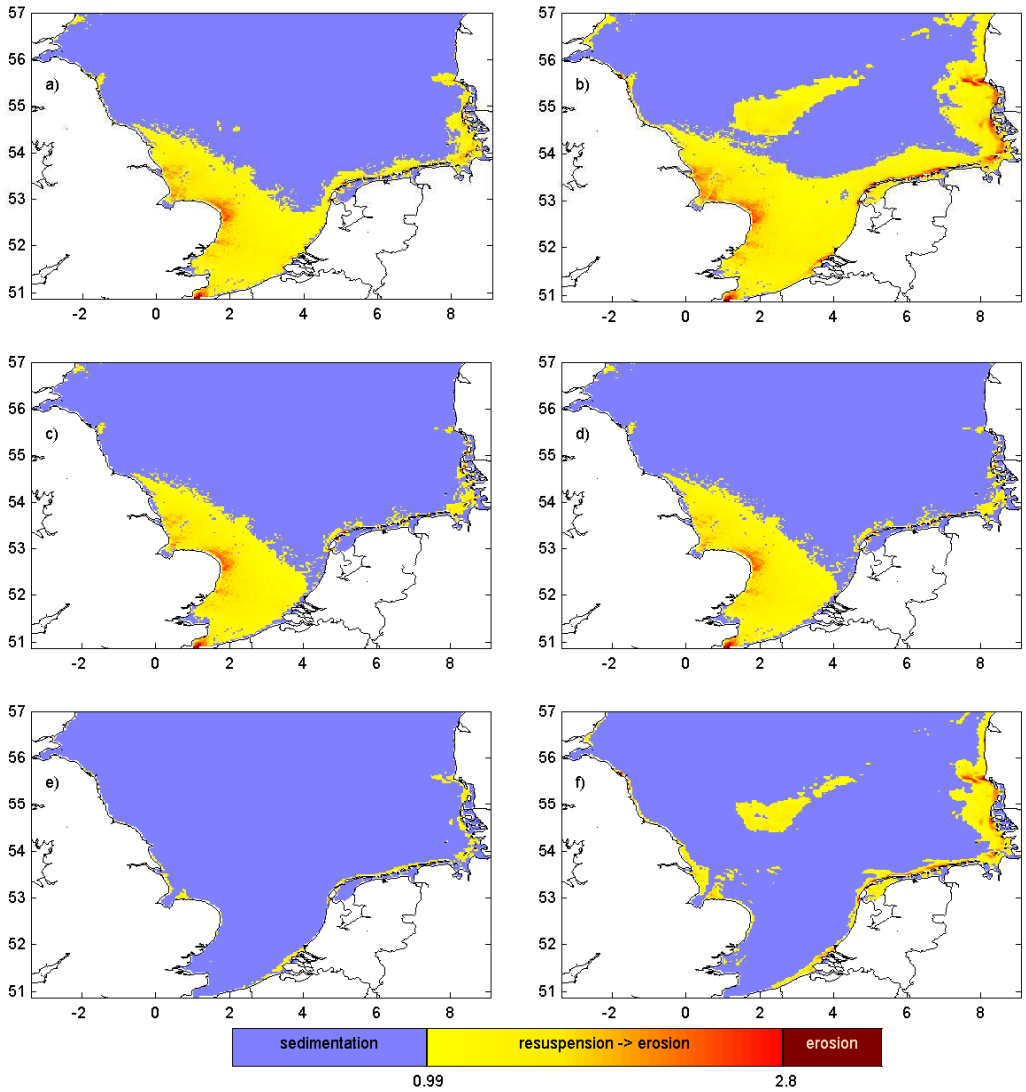

Figure 4.3: Seasonal mean total shear stress velocity (a, b) and its components due to currents (c, d) and waves (e, f) during calm (left) and storm (right) periods in 2002.

With the increasing of the frequency of the storm events in the North Sea, new zones with high surface SPM concentration occur (Fig. 4.3f). The location of these zones is mainly determined by the topography. The energy of the waves coming from the North Atlantic dissipates mainly in the shallow regions, such as the Dogger Bank and the German Bight. This energy results in the increase of V^* , which is high enough for the resuspension. Generally, the resuspension zone during the storm period covers the southern part of the model area, shallow areas in the open North Sea and most of the German Bight.

The increase in the V^* leads to erosion, but the seasonal mean V^* distributions do not show permanent erosion zones, because the erosion events have a short duration and are rare (as shown in Section 5.3). The erosion zones occur when V^* exceeds the red zone in the resuspension interval (Fig. 4.3) and reaches the threshold value V^*_{ero} located in the regions with a combination of high V^*_{cur} and V^*_{wave}.

The topography explains also the occurrence of sedimentation zones in the North Sea. They are located mainly in the deep parts of the North Sea, where the currents and wave induced shear stress in the near-seabed layer is not high enough to keep SPM in suspension. The sedimentation zones cover the open part of the model area, excluding the Dogger Bank region during the storm period. In contrast to the erosion, seasonal mean values of V^* clearly define sedimentation zones, because hydrodynamic conditions in the deep North Sea do not differ during calm and storm periods in the near seabed water layers.

Chapter 5

Dynamics and spatial distribution of SPM in the North Sea

This chapter presents results of model simulations which were carried out for the years 2002 and 2003 with a time step of 5 min. Model results were stored as hourly or 20 minutes averaged three-dimensional values of (1) SPM concentration in water and (2) fine sediment mass in the seabed for each of the three SPM fractions (see Section 2.2.2). Here modeled seawater SPM concentrations and the seabed mass of fine sediment are presented as the sum of all three fractions. Model results are compared with total suspended matter (TSM) concentrations retrieved from satellite data (see Chapter 3) and with in-situ measurements of the inorganic suspended matter (ISM) and the total suspended matter concentrations collected during several cruises at the sea surface (Section 5.1) and in the water column (Section 5.2). Section 5.3 analyzes time series of SPM concentrations in different locations in the North Sea and compares them to time series of the major forcing factors, i.e. the wind speed, significant wave height and shear stress velocity. Section 5.4 discusses temporal and spatial evolution of fine sediment in the seabed. Analysis of the dynamics of fine sediment mass in seawater and in the seabed (Section 5.5) conclude this chapter.

5.1 Horizontal SPM distributions

5.1.1 Modeled surface SPM concentrations

Based on the meteorological conditions and waves in the North Sea, one can distinguish two periods with different SPM distribution patterns further on named as the calm period typically occurring during the warm season (from 15 April to 15 October) and the storm period occurring during the cold season (from 15 October to 15 April). Seasonal mean surface SPM concentrations in the year 2002 and 2003

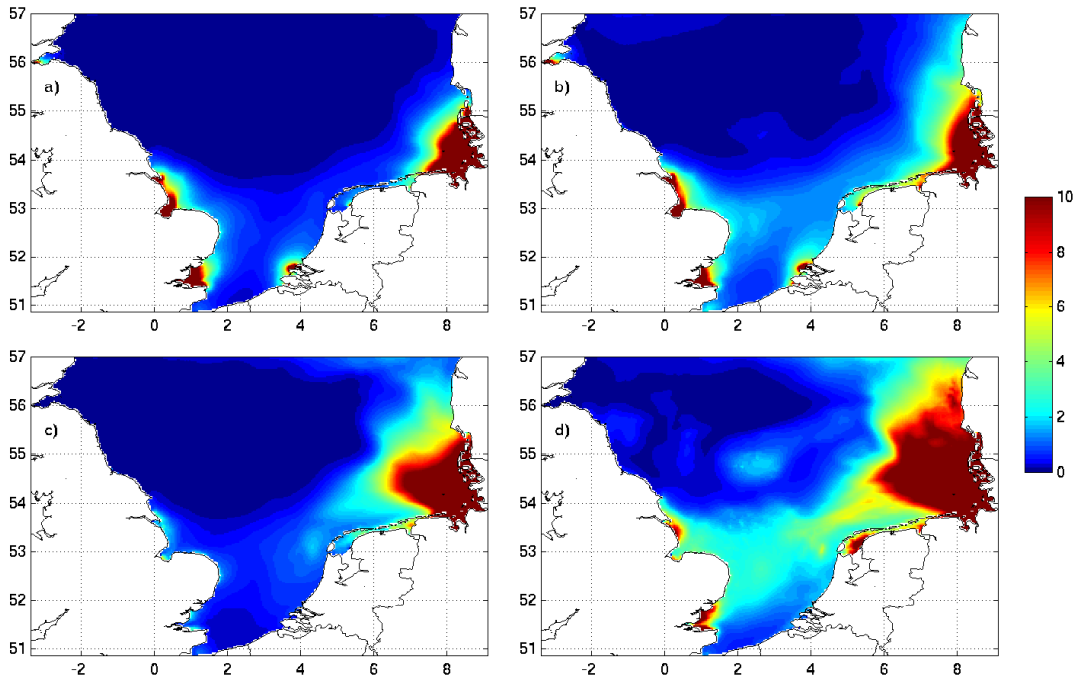

Figure 5.1: Seasonal mean modeled SPM concentrations ($mg\ l^{-1}$) in 2002 and 2003 averaged for the warm period (15 April - 15 October, a and c) and for the cold period (15 October - 15 April, b and d).

for the calm and the storm periods are shown in Figure 5.1. SPM plumes may develop under both storm and calm conditions. The initial distribution of fine sediment in the bottom (Fig. 2.3) shows regions where high SPM concentrations at the sea surface potentially occur.

Under calm conditions, sea currents redistribute the SPM and determine the

location of zones with permanent high horizontal gradients of SPM concentration (SPM fronts) near the coast, close to river mouths and near the English cliffs (Fig. 5.1a). The seabed-water exchange processes are always intensive in the shallow German Bight, also under calm conditions. At these depths (up to 25 m) even small perturbations due to currents and waves increase the SPM concentration in the bottom water layer due to resuspension and erosion. The vertical mixing is sufficient to redistribute high SPM concentrations ($> 10\ mg\ l^{-1}$) from the bottom to the sea surface. Additionally, the German Bight is supplied by SPM from rivers, mostly from the river Elbe (Fig. 2.4). Note, that in 2003 the rivers influence on surface SPM concentration is not significant, because of the low discharge and SPM load. Vertical mixing in the German Bight dominates the horizontal advection of fluvial SPM, even close to river mouths, thus maintaining visible fronts near the coast. These SPM front propagates northwards parallel to the coast following the commonly observed counter-clockwise general circulation pattern in the North Sea (e.g. Pohlmann and Puls (1994)). During the storm period, strong water-seabed exchange and mixing of SPM in the water column result in the expansion of the relatively high SPM concentrations further into the open North Sea (Fig. 5.1b). The maximum of surface SPM concentrations still remains near the coast.

Generally, during the warm period in the year 2003 due to higher significant wave height in comparison to 2002 (see Section 4.2), the vertical mixing keeps more SPM in suspension in seawater and leads therefore to the higher surface SPM concentration also during cold period in 2003.

5.1.2 Comparison between modeled and measured surface SPM concentrations

The water samples were collected during several cruises in 2002 in the eastern and south-eastern North Sea (Fig. 2.3). A direct comparison of model results with observational data was only possible for the GKSS data-set (Table 5.1), because sample processing allowed obtaining inorganic suspended matter (ISM) fraction separately from the total suspended matter (TSM) concentrations. The water samples were processed using gravimetric filter analysis of TSM (Strickland and

Table 5.1: Summary of SPM in-situ data for the year 2002 used for the evaluation of model results (range and mean of measured and modeled SPM concentrations).

Date-set		1	2	3
Months of sampling		4,5	1, 2, 8, 9	3,11
Number of stations		46	105	34
Depths range		$1-36m$	$8-12m$	$0.5m$
Cruise organizer		GKSS[1]	BSH[2]	NLOE[3]
Parameter		ISM	TSM	TSM
Measurements, $mg\ l^{-1}$	range	0.00-20.40	0.44-243.86	20.00-140.00
	mean	2.07	7.88	63.21
Model range, $mg\ l^{-1}$	range	0.02-40.27	0.03-240.35	10.44-74.74
	mean	7.91	19.20	29.86

[1]GKSS Research Centre
[2]Federal Maritime and Hydrographic Agency
[3]Niedersächsisches Landesamt für Ökologie

Parsons, 1998; der Linde, 1998) and gravimetric filter analysis for ISM and organic suspended matter (OSM) (Hirota and Szyper, 1975). Generally the model is in good agreement with all observations from the data-set 1 (Table 5.1; Fig. 5.2) with a correlation coefficient (see Appendix 7.2 and von Storch and Zwiers (1999)) of 78% and BIAS (Model-measurements) of 5.5 $mg\ l^{-1}$.

The TSM concentrations in data-set 2 and data-set 3 were measured without separating the organic and inorganic fractions (Table 5.1; Fig. 5.3). Depending on the season and location OSM fraction in the North Sea can vary from about 20% of the TSM concentration in January in the southern part of the North Sea up to 50% in June in the Skagerrak (Eisma and Kalf, 1987). The model results correlates well with the measurements from the data-sets 2 and 3, because in the periods from January to March and from August to November when measurements were conducted, the OSM fraction is relatively small (Moll, 1998). Data-sets 2 and 3 include measurements from the very shallow locations ($< 5m$). With the horizontal resolution of about 3 km and the vertical resolution of about 5 m the model is not capable of detailed resolution of SPM processes in very shallow coastal regions. Therefore, only points with the minimum depth of $5m$ and located

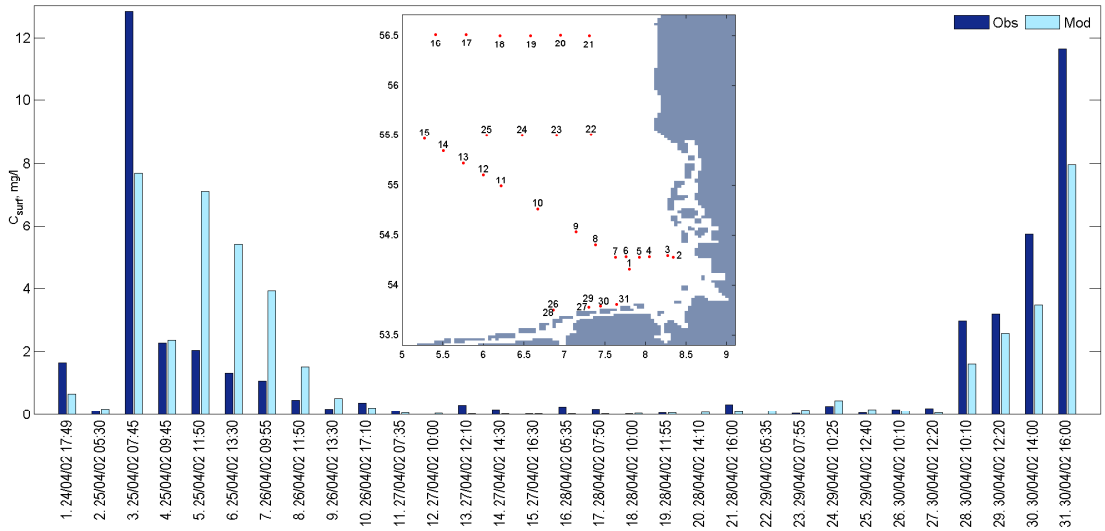

Figure 5.2: Measured and modeled surface SPM concentration ($mg\ l^{-1}$) in the North Sea at selected locations from the data-set 1 (Table 5.1).

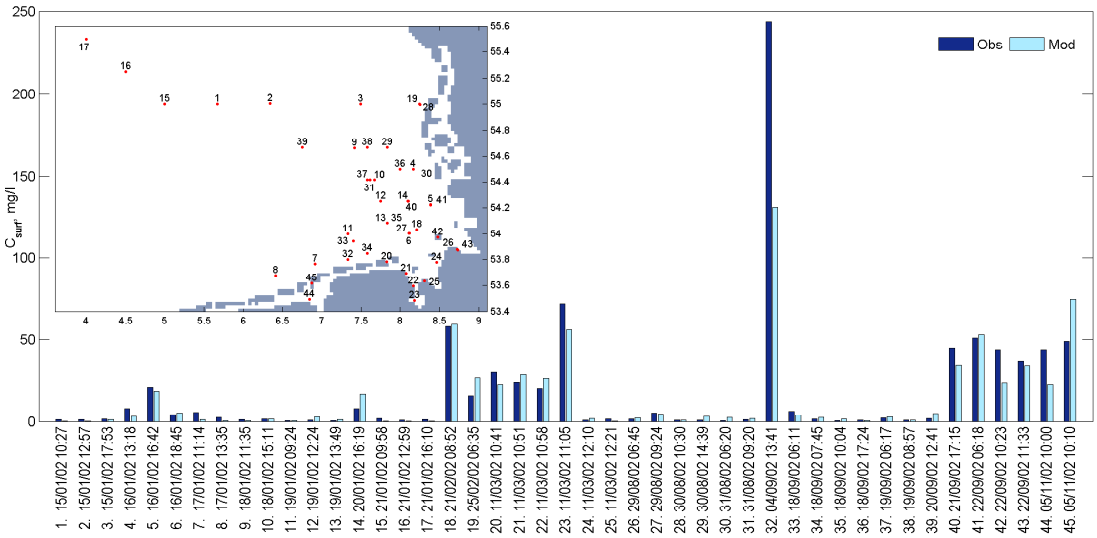

Figure 5.3: Measured and modeled surface SPM concentration ($mg\ l^{-1}$) in the North Sea at selected locations from the data-set 2 and data-set 3 (Table 5.1).

approximately 6 km (two model grid cells) away from the coast were selected for comparison. The correlation coefficient between measurements (data-sets 2 and 3) and the model results for these selected points is 92%, with a BIAS value of 3.1 $mg\ l^{-1}$ (Fig. 5.3). The correlation coefficient for all TSM measurements in the data-sets 2 and 3 is lower (40%, BIAS = 3.9 $mg\ l^{-1}$).

Two types of satellite data obtained from MERIS (medium-spectral resolution, imaging spectrometer operating in the solar reflective spectral range; Fig. 5.4) and MOS (Modular Optical Spectrometer; Fig. 5.5) are used for the comparison with modeled surface SPM concentrations. The data derived from MOS is produced by the German Aerospace Center (DLR, 2007). MERIS data is processed using the MERIS Case-2 Regional Processor (Doerfer et al., 2006) to calculate SPM concentrations at the sea surface (see Section 3.2 for details). MERIS scenes were selected so that they cover possibly largest parts of the modeling domain (Fig. 5.4). MERIS scenes are shown without the quality control system application (Section 3.3) in order to keep large spatial coverage. Although the model captures general horizontal SPM pattern found in MERIS data, the SPM fronts in the satellite data are weaker compared to the model results. SPM concentrations derived from satellite data have a cut-off maximum value ($\approx 70\ mg\ l^{-1}$ for MERIS data), due to general constraints in the processing algorithms. Therefore satellite data may not be able to resolve larger gradients in zones with high SPM content, i.e. in the SPM fronts. MOS scenes were selected to show the SPM surface distributions during storm periods, e.g. in January 2002. MERIS data in this period is not available. Because storms are frequently accompanied by cloudy weather, these scenes (Fig. 5.5) only partially cover the model domain. MOS scenes on January 28 2002 (Fig. 5.5g) captures high surface SPM concentration in the German Bight induced by additional wave influence during the storm.

Modeled SPM concentration pattern at the surface resembles the seabed SPM distribution (cf. Fig. 5.4b, Fig. 5.5b and Fig. 2.3). SPM concentrations retrieved from satellite data (Fig. 5.4a, Fig. 5.5a) show the same horizontal distribution pattern. Modeled values are represented by the concentration in the upper model layer (with the thickness of about 5 m). Satellite data is integrated over the signal penetration depth. The quantitative comparison between the modeled and satellite data is difficult due to the different definitions of the "surface" and because filtering of unrealistically high values of surface SPM concentration is needed. In contrast to SPM fields derived from satellite data, the modeled SPM surface distributions do not capture fine details in the horizontal patterns due to numerical diffusion effect.

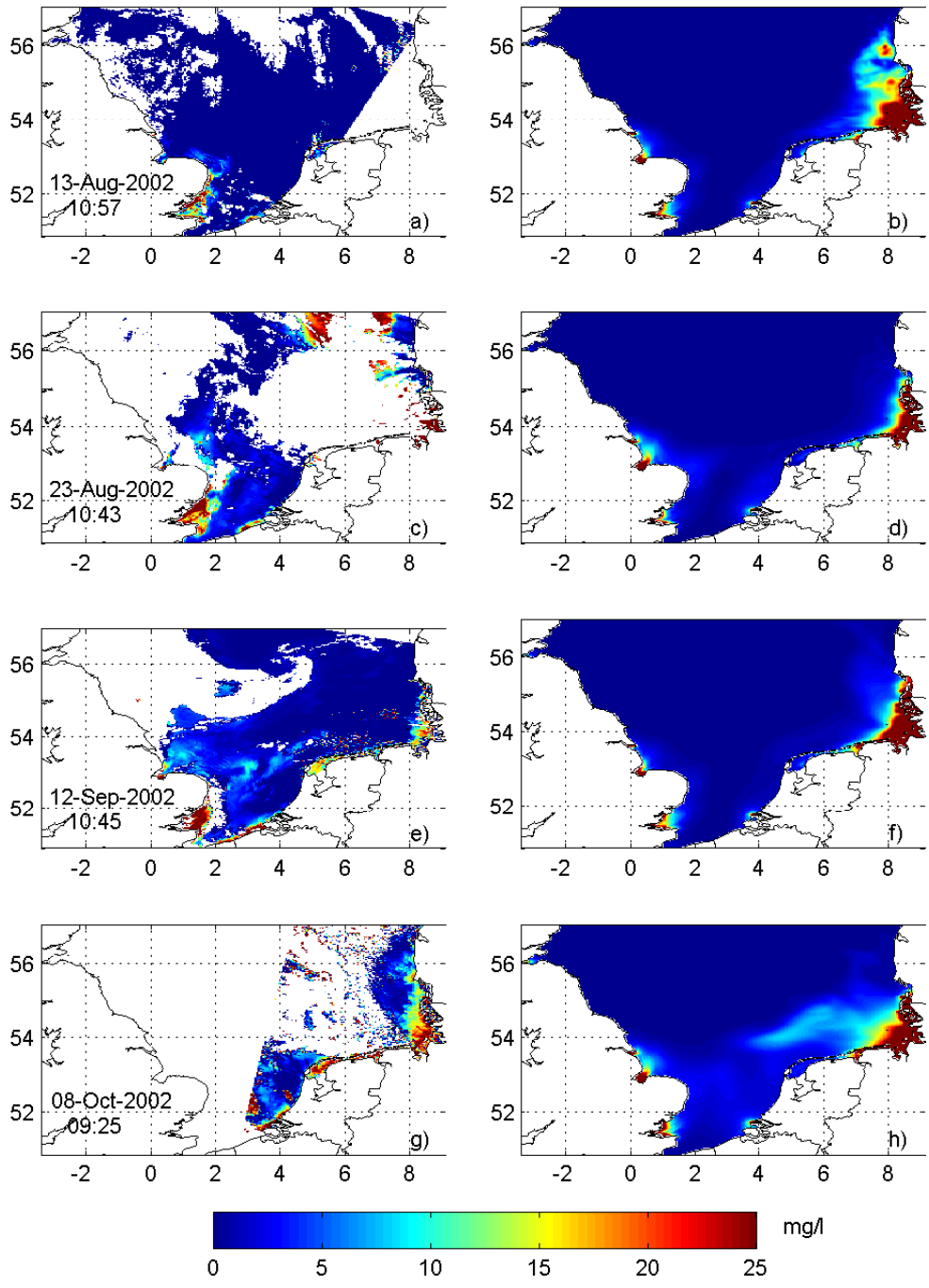

Figure 5.4: Surface SPM concentration ($mg\ l^{-1}$) in the North Sea calculated from MERIS data (left) and by the model (right) in August, September and October 2002.

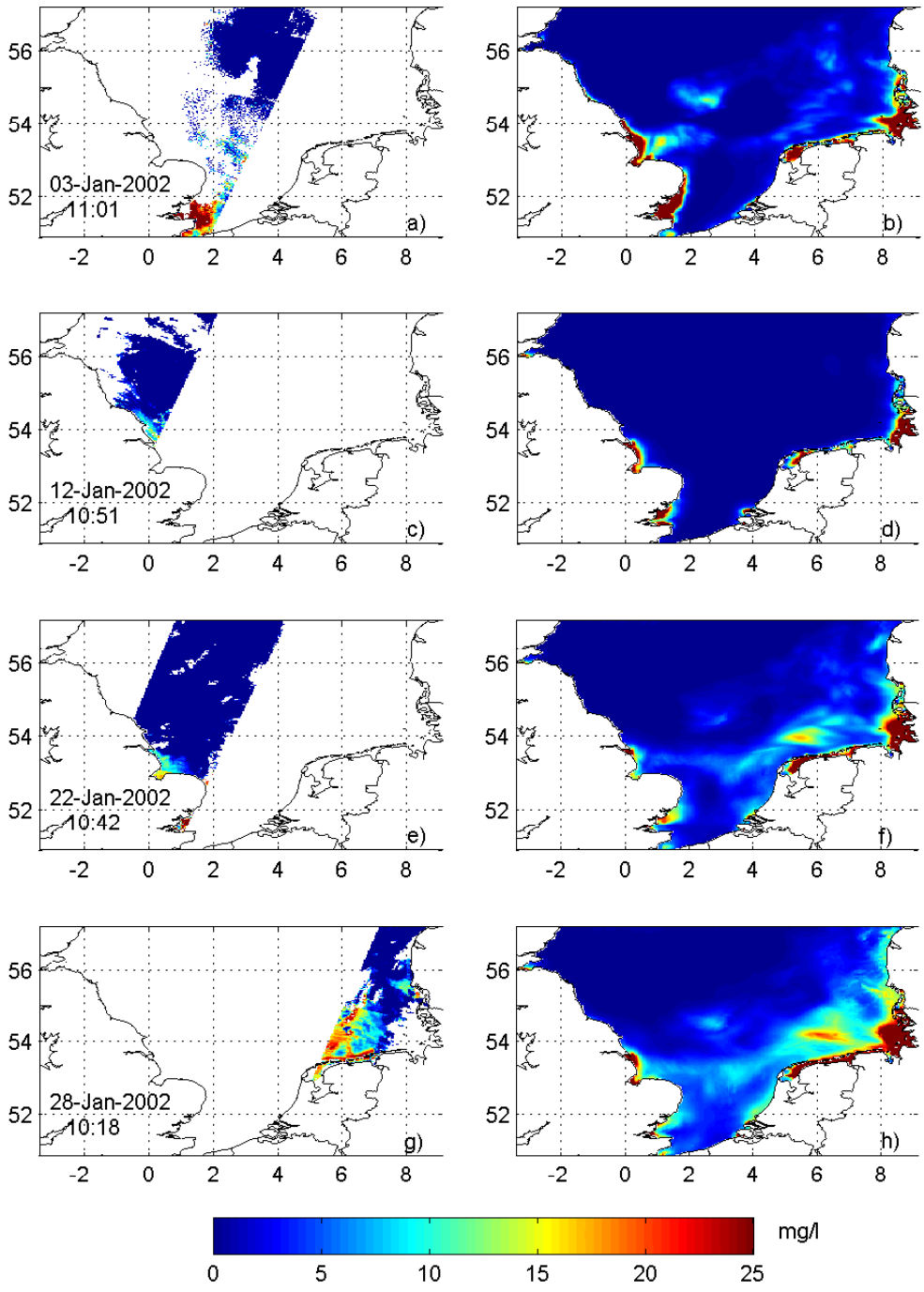

Figure 5.5: Surface SPM concentration ($mg\ l^{-1}$) in the North Sea calculated from MOS data (left) and by the model (right) in January 2002.

5.2 Vertical SPM distributions

5.2.1 Modeled SPM concentrations in the water column

Vertical distributions of SPM in the North Sea vary from full mixing over the entire water column to strong stratification. For the vertical SPM distribution analysis, a vertical section along $3°E$ (Fig. 2.3) is choosen as it includes circulation patterns common for the different regions of the North Sea (i.e. off-shore, coastal, close to the estuaries, and in the passage of water entering from the English Channel). The vertical sections show two representative seasonal distributions (see Section 5.1) of vertical SPM concentrations in January and July of 2002 (Fig. 5.6) with the typical for the calm and storm period values of wind speed and significant wave height (Fig. 5.6a and e). Opposite to calm conditions in July, with the section mean wind speed of 7.0 $m\ s^{-1}$ and significant wave height of 0.8 m, the section mean value of wind speed reaches 22.5 $m\ s^{-1}$ and significant wave height reaches 6.7 m during the storm in January.

Due to frequent storms during winter time accompanied by high waves up to $10m$ (Fig. 5.6a), the shear stress velocity (V^*) often exceeds the threshold values of resuspension and erosion, e.g. the mean value of V^* along the vertical section is 0.031 $m\ s^{-1}$ in January (Fig. 5.6d). During the storm in January 2002, shear stress velocities exceeded the erosion threshold ($V^* > V^*_{ero}$; Fig. 5.6d) almost along the entire section. The wave component (V^*_{wave}) dominated the shear stress velocity everywhere with the exception of the region near the English Channel, where the shear stress component due to currents (V^*_{cur}) is higher. Erosion events remove fine sediment from the bottom down to the erosion depth of up to 9 mm in the Dogger Bank (around $55 \circ N$; Fig. 5.6c). High SPM concentrations (20-25 $mg\ l^{-1}$; Fig. 5.6b) are found near the seabed in locations where the content of fine sediment in seabed is high. Vertical mixing leads to redistribution of SPM from lower to upper layers. The SPM concentrations at the sea surface is > 15 $mg\ l^{-1}$.

When turbulence is not strong enough to keep the particles in suspension, they settle at the bottom. In summer, the model shows relatively high SPM mass in the uppermost seabed layers (Fig. 5.6g). SPM accumulated in seawater during storm

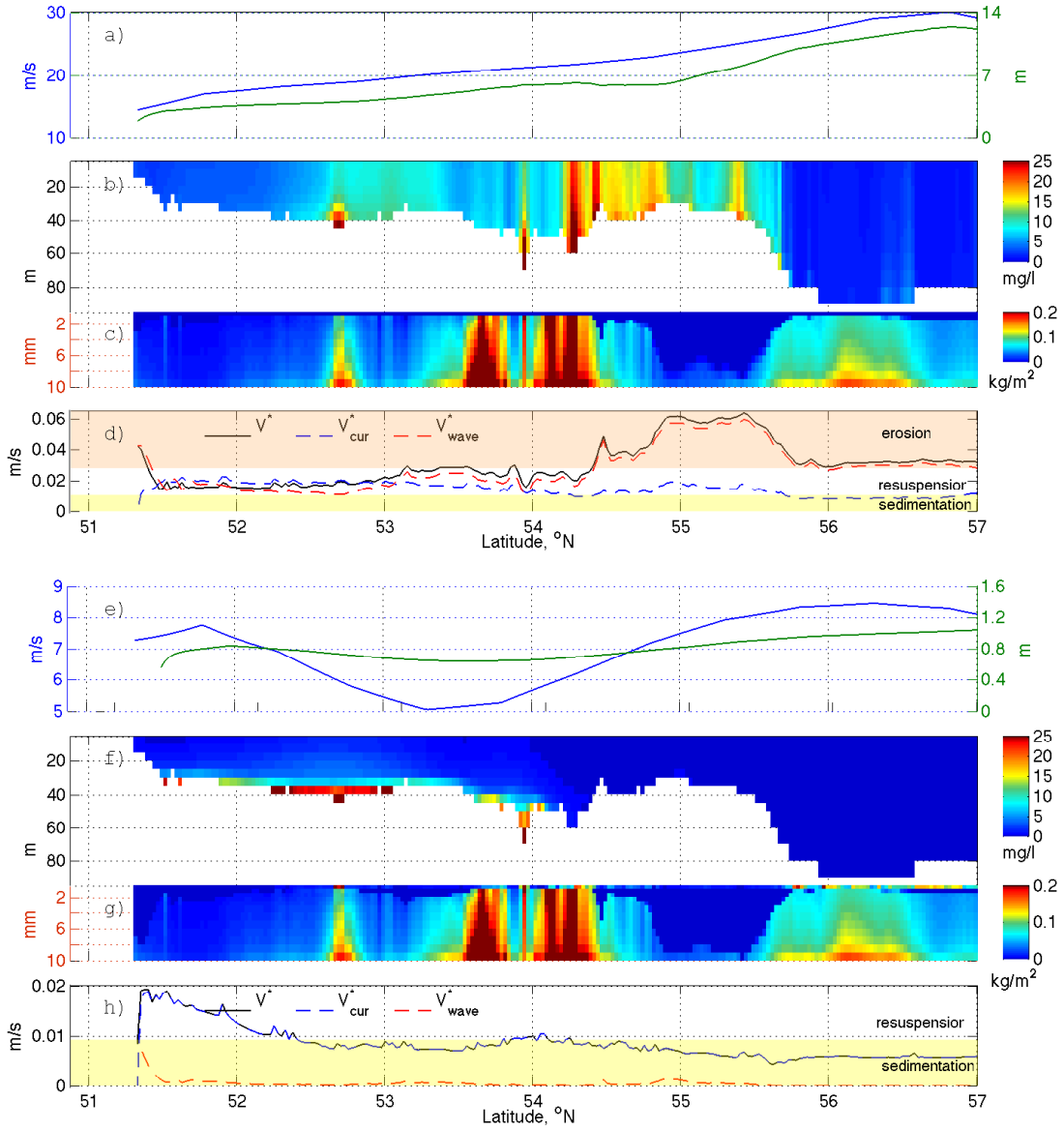

Figure 5.6: Vertical sections from South to North along $3°E$ of modeled SPM concentration ($mg\ l^{-1}$) in the water b) and f), sediment mass ($kg\ m^{-2}$) in the upper $10mm$ of the seabed c) and g) in January and July 2002 and corresponding shear stress velocity V^* ($m\ s^{-1}$) d) and h) with its components due to waves (red) and currents (blue); threshold values of V^* for erosion, resuspension and sedimentation are indicated by colored areas. Corresponind wind speed ($m\ s^{-1}$) a) and e) (blue) and significant wave height (green) are shown.

periods, sinks into the bottom model layers and starts to deposit into the seabed (Fig. 5.6f and g). The shear stress velocities are generally below the resuspension threshold (the mean value of V^* along the section is $0.008\ m\ s^{-1}$). In the calm

periods the contribution of V^*_{wave} is not essential (Fig. 5.6h). Resuspension occurs only near the English Channel ($51.4° - 52.3°N$) because of the higher currents velocity in this area. Despite the resuspension, the SPM concentration at the sea surface is low (about 1-2 $mg\ l^{-1}$; Fig. 5.6f) because the content of sediment in seabed is also low ($< 0.1\ kg\ m^{-2}$; Fig. 5.6g) and additional wave forcing (wave height about $1m$) is not strong enough to redistribute SPM in the water column (Fig. 5.6e).

Generally, sedimentation occurs in the deeper areas of the North Sea ($> 30m$). Exchange processes between the bottom water layer and the upper seabed layers are slow during the calm period. This enables the horizontal advection to redistribute SPM forming zones of high SPM concentrations in the bottom water layers (20-25 $mg\ l^{-1}$; Fig. 5.6f). Sedimentation adds sediment mass in the uppermost seabed layer (Fig. 5.6g). Due to bioturbation, sediment redistributes slowly to the deep layers in the seabed.

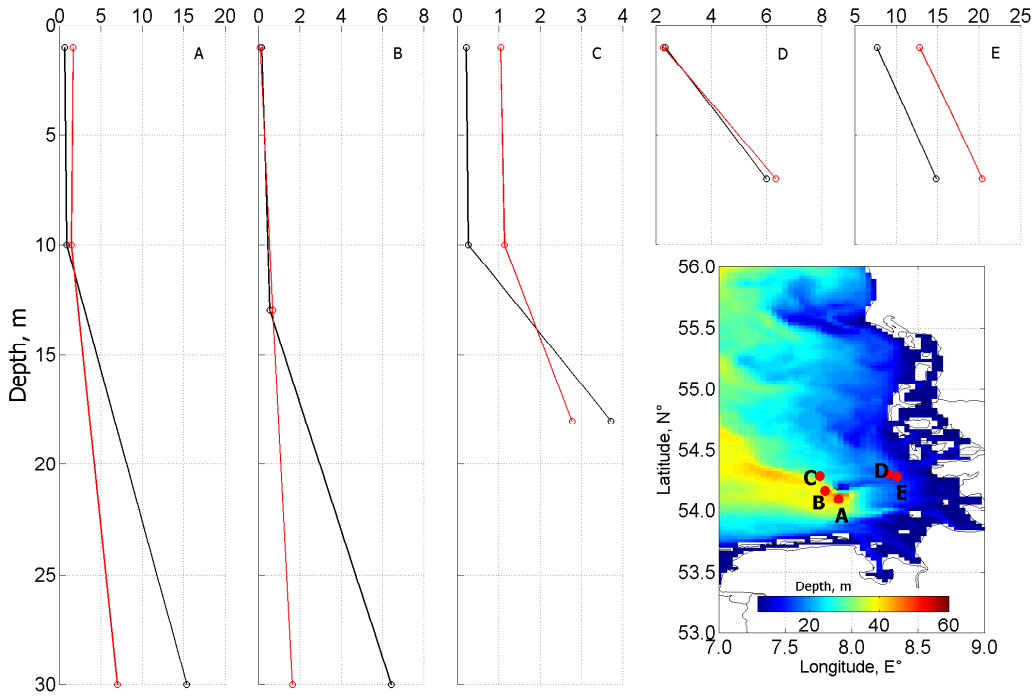

Figure 5.7: Observed (red) and modeled (black) SPM concentrations ($mg\ l^{-1}$) at locations A,B,C,D and E in the German Bight in April 2002.

5.2.2 Comparison between modeled and measured SPM concentrations in the water column

Model results are compared with available in-situ measurements (Table 5.1). Model results suggest that under calm conditions the SPM concentration increases towards the bottom with the maximum in the bottom water layer. Such distribution is caused by gravitational sinking and resuspension (Fig. 5.7; locations A, B and C). Measured SPM concentrations range from 0.5 to 1.5 $mg\ l^{-1}$ in the surface layer and from 3 to 15 $mg\ l^{-1}$ in the lowest layer. Modeled SPM concentrations are up to 2.2-8 $mg\ l^{-1}$ in the surface layer and up to 8-15 $mg\ l^{-1}$ in the bottom water layer close to the coastal SPM front (see Section 5.1) and in the shallow regions, such as in the locations D and E (Fig. 5.7).

The model is generally in good agreement with measurements especially in the surface layers and reproduces the vertical profiles of the observed SPM concentration. The model overestimates SPM concentration in the bottom layers. One explanation is the flocculation process (when fine particulates are caused to clump together into flakes). When the SPM concentrations are high the flocculation increases the particle size and settling velocity according to Stokes' Law, laboratory experiments (e.g. Asaeda and Wolanski (2002)) and in-situ measurements (Dyer et al., 1996). Subsequently it increases the sedimentation rate (Section 2.1.4). As a result, more SPM will be removed from the bottom water layer. This process is not included in the current model configuration and may explain the overestimated SPM concentrations in the bottom water layer.

5.3 Time series of SPM concentrations and mass

Figure 5.8 shows the dynamics of modeled surface SPM concentration in different locations in the years 2002 and 2003. During the simulation period the strong seasonality of SPM surface concentration is seen in the location L3, L4 and L5. The minimum of surface SPM concentration occurred in the summer time and maximum during the cold period. In the location L1 in the German Bight the seasonality is not so pronounced, because the currents component play significant

role in the shear stress velocity and do not change from warm to cold periods in this area. The shear stress and vertical mixing due to currents are strong enough to keep SPM in suspension under such conditions.

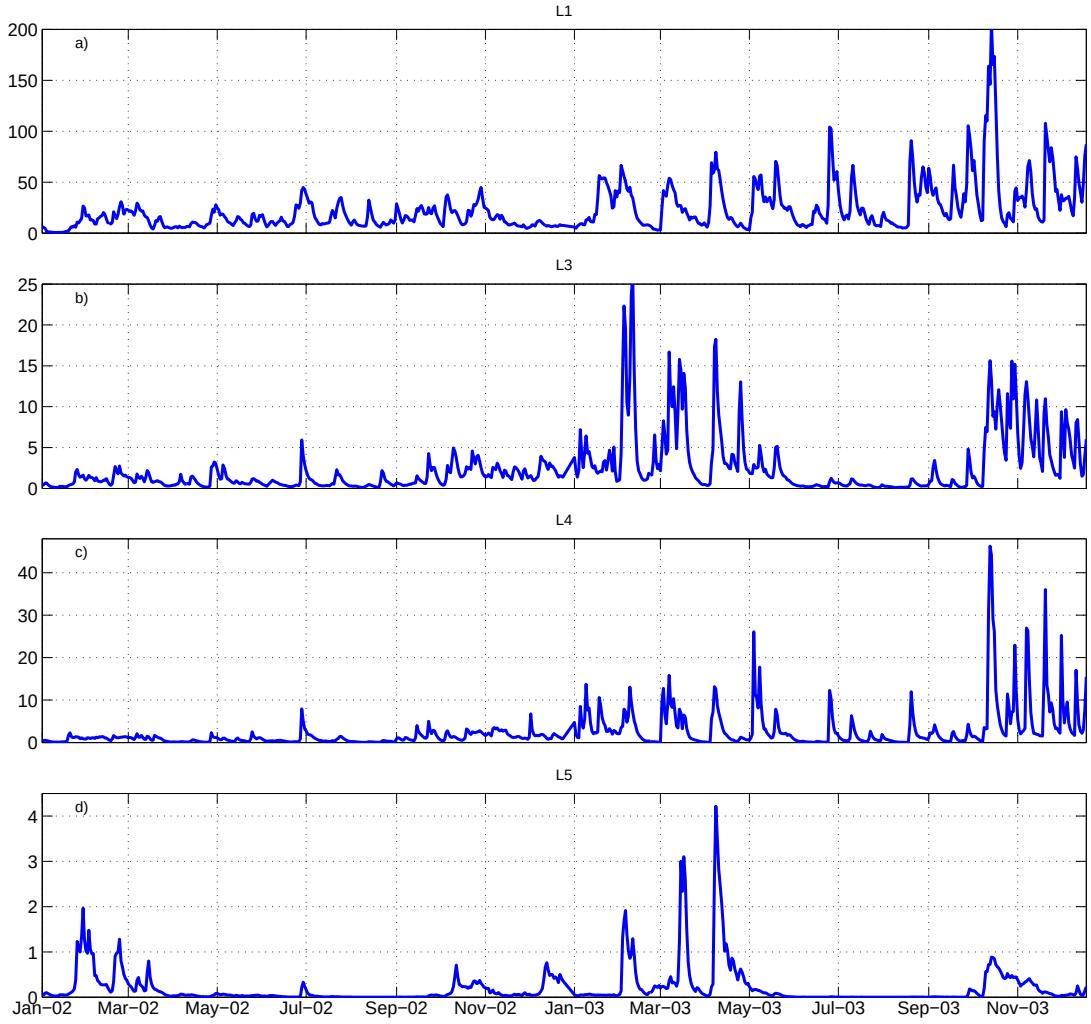

Figure 5.8: Time series of daily averaged surface SPM concentration ($mg\ l^{-1}$) in the locations L1, L3, L4 and L5 (see Fig. 2.3 for the geographical locations) in the years 2002 and 2003.

Time series of daily averaged surface SPM concentrations smooth the instance SPM dynamics which can be capture by the model. Therefore the time series at six locations in the year 2002 were selected (Table 5.2) to show in details the different temporal evolution of SPM concentrations (Fig. 5.9 and Fig. 5.10). The selected locations illustrate the dynamics of SPM concentrations under different

conditions (i.e. waves or currents regimes) and in different regions (i.e. shallow or deep water, influenced by fluvial SPM or by cliffs erosion).

The time series of shear stress velocity at locations L1, L2, L3, L4, L5 and L6 (Fig. 5.9d, h, i and Fig. 5.10d, h, i) capture the period of the spring-neap tide cycle. The vertical mixing in this points, especially in L2 and L5 was not strong enough to redistribute the SPM concentration from the bottom water layer to the surface producing large vertical difference of about 40 $mg\ l^{-1}$. Despite the similar depth, the SPM concentrations in the bottom water layer in locations L2 and L5 are different (2 - 10 $mg\ l^{-1}$ and 20 - 40 $mg\ l^{-1}$ respectively) even during the stormy period from January through March characterized by the wind speed of $> 20\ m\ s^{-1}$ and significant wave height (Hs) of up to 6 m (Fig. 5.9f, g and Fig. 5.10f, g). This difference is attributed to the lower content of fine sediment in the seabed in L2 compared to L5 (Table 5.2). The peak of the storm in the end of January leads to a small increase in the surface SPM concentration at L5 (from near 0 $mg\ l^{-1}$ to about 3 $mg\ l^{-1}$) and at L2 (up to 0.5 $mg\ l^{-1}$). In the both locations variations of SPM concentration in the bottom water layers are caused mainly by the resuspension with the value of the annual mean shear stress velocity (V^*_{mean}) 0.59 $cm\ s^{-1}$ at L2 and 0.98 $cm\ s^{-1}$ at L5. In contrast to the SPM concentrations in the bottom water layer, the surface SPM concentrations at these two relatively deep locations are very close in magnitude (around 0.01 $mg\ l^{-1}$) because the influence of waves on the vertical mixing is not very strong (see Fig. 5.9e and Fig. 5.10e; Table 5.2).

The circulation patterns in the North Sea with high current velocities in shallow and coastal regions lead to the formation of zones with very low fine sediment content in the seabed, for example near English cliffs in the location L3 (Fig. 5.9i). In addition to washout of fine sediment, the deposition of SPM is hardly possible in these areas. The highest of annual mean shear stress velocity of 1.6 $cm\ s^{-1}$ is observed in the location L3, generated mainly by currents. High shear stress velocities often exceeding the threshold value for erosion (Fig. 5.9l) keeps the eroded and advected SPM in suspension, leading to a high annual mean SPM concentration ($> 25\ mg\ l^{-1}$) in the near-bottom layer.

In shallow regions of the North Sea, currents and waves may become equally

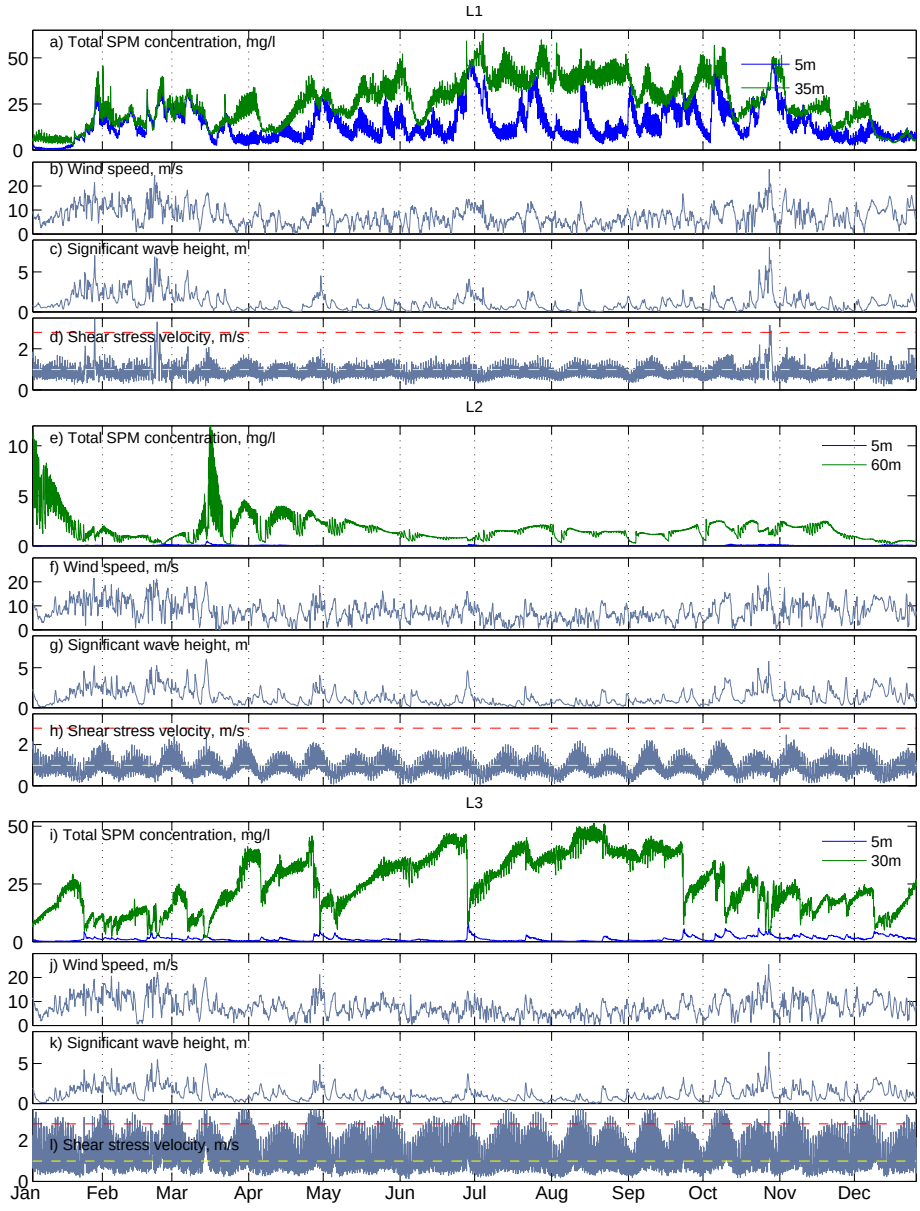

Figure 5.9: Calculated time series of SPM concentrations ($mg\ l^{-1}$) in the North Sea in 2002 at locations a) L1, e) L2 and i) L3 in the surface layer (blue line) and in the near bottom water layer (green line), and corresponding wind speed ($m\ s^{-1}$; b, f and j), significant wave height (m; c, g and k) and shear stress velocities ($cm\ s^{-1}$; d, h and l) with threshold values V^*_{res} (yellow dashed line) and V^*_{ero} (red dash line).

important leading to a stronger vertical mixing. Although points L1 and L4 are located in the shallow regions, the mean annual SPM concentrations are different (Fig. 5.9a and 5.10a), at the surface and in the bottom water layer. The concentrations are 13.92 $mg\ l^{-1}$ at the surface and 25.79 $mg\ l^{-1}$ in the bottom layer of L1

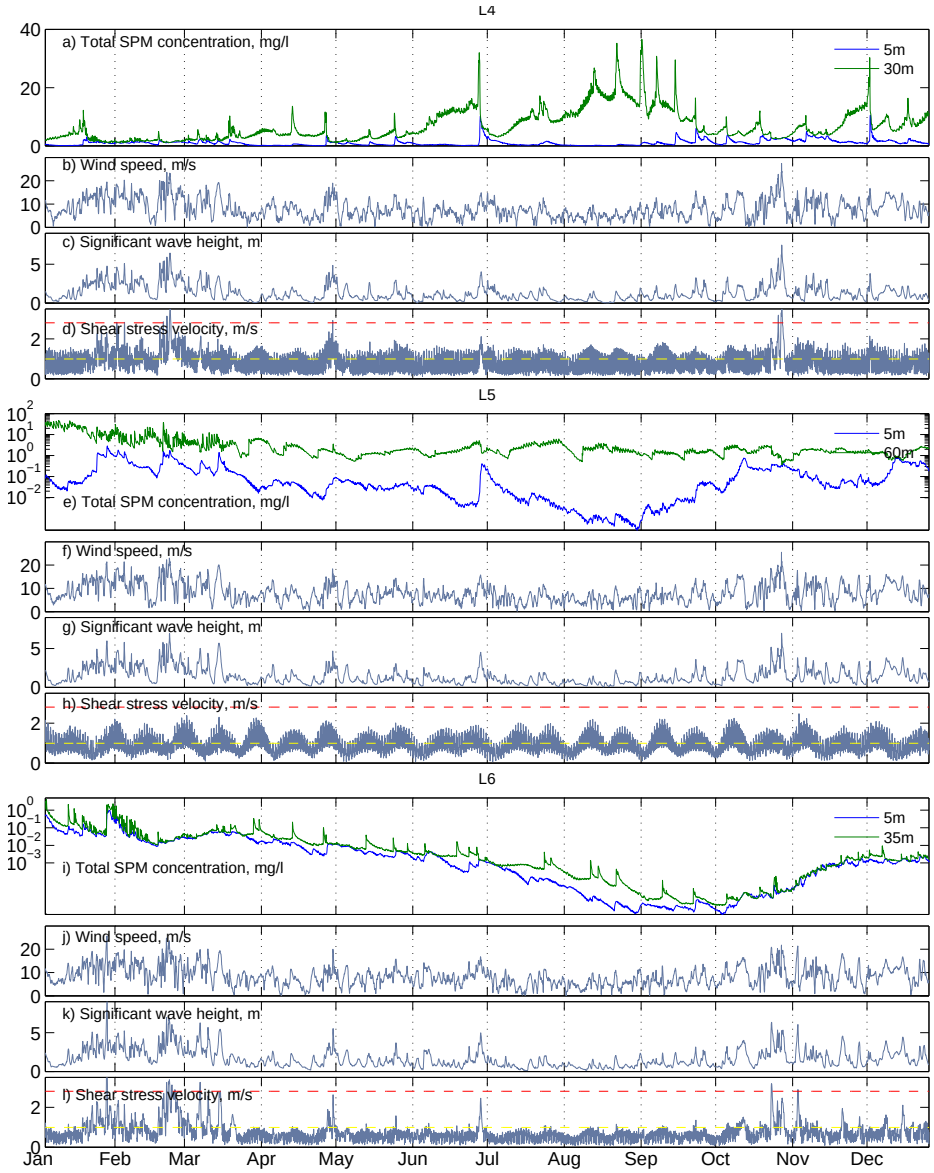

Figure 5.10: Calculated time series of SPM concentrations ($mg\ l^{-1}$) in the North Sea in 2002 at locations a) L4, e) L5 and i) L6 in the surface layer (blue line) and in the near bottom water layer (green line), and corresponding wind speed ($m\ s^{-1}$; b, f and j), significant wave height (m; c, g and k) and shear stress velocities ($cm\ s^{-1}$; d, h and l) with threshold values V^*_{res} (yellow dashed line) and V^*_{ero} (red dash line).

and 1.04 $mg\ l^{-1}$ at the surface and 6.80 $mg\ l^{-1}$ in the bottom layer of L4. This is explained by the much higher fine sediment content of 43.63 % in the seabed at L1 compared to 0.73 % at L4 (see Table 5.2). During calm periods (July-October) the influence of currents on V^* is dominant and the wave components are not essential in these locations. Under such conditions the turbulent diffusion is not

Table 5.2: Model grid points used to analyze annual time series of SPM, their locations, depths, range, annual mean SPM concentrations (C_{mean}) in the surface layer and in the bottom model layer, annual mean shear stress velocity (V^*_{mean}) and initial content of fine sediment in the seabed (f_{fine}).

Location	Geographical position	Depth, m	Surface, $mg\ l^{-1}$			Near seabed, $mg\ l^{-1}$			V^*_{mean}, $cm\ s^{-1}$	f_{fine}, %
			C_{min}	C_{max}	C_{mean}	C_{min}	C_{max}	C_{mean}		
$L1$	$54.15^oN, 07.98^oE$	39	0.32	48.97	13.92	0.77	63.25	25.79	0.91	43.62
$L2$	$54.55^oN, 00.65^oE$	61	0.01	0.49	0.16	0.11	15.69	3.95	0.59	2.44
$L3$	$53.07^oN, 01.98^oE$	35	0.08	8.49	1.21	0.39	51.40	25.21	1.60	0.83
$L4$	$53.07^oN, 04.27^oE$	32	0.03	10.52	1.04	0.32	36.57	6.80	0.89	0.73
$L5$	$54.07^oN, 02.81^oE$	60	3e-4	2.86	0.04	0.16	47.18	1.75	0.98	10.30
$L6$	$55.45^oN, 02.81^oE$	36	1e-4	1.26	0.03	4e-4	8.38	0.06	0.76	2.26

strong enough to redistribute the SPM homogeneously in the water column so that the vertical stratification is formed. The difference of SPM concentrations between the surface and the near bottom water layer is high, up to 50 $mg\ l^{-1}$ in L1 and 35 $mg\ l^{-1}$ in L4. The SPM concentration in the bottom water layer correlates with the shear stress velocity with the correlation coefficient of up to 85% in L1 during the calm period (from 20.09.2002 to 03.10.2002). The shear stress velocity continuously exceeded the threshold value for resuspension (Fig. 5.9d and 5.10d) causing the resuspension to add to the SPM burden in the water column. Additional wave forcing during stormy periods in January-March and October-November (with the wind speed of $> 12\ m\ s^{-1}$ and Hs of up to 5 m; Fig. 5.9b and c and Fig. 5.10b and c) results in strong vertical mixing of SPM. During January, February and October, the values of V^* often exceeded V^*_{res} and sometimes even V^*_{ero} . Consequently, the SPM concentrations increased from 8 to 25 $mg\ l^{-1}$ at L1 and reach 2 $mg\ l^{-1}$ at L4 (both, in the surface and in the bottom water layers) after the first erosion event in the end of January (Fig. 5.9d and 5.10d). Currents and waves remained strong enough to exceed V^*_{res} also in February and March. The next erosion event in the end of February did not play a significant role in changing the SPM concentrations because the mass eroded in January was still in suspension and the content of fine sediment in the seabed was low. The next erosion event occurred in the end of October in both locations. At L1 erosion and strong vertical mixing formed high SPM concentrations (up to

45 $mg\ l^{-1}$) in the whole water column. At L4 erosion is not so dramatic because of the lower content of fine sediment in the seabed. Under calm conditions later in the year, sinking and sedimentation lead to the formation of large vertical gradients in the SPM concentration. The maximum of the SPM concentrations in the bottom water layer occurs end of June (60 $mg\ l^{-1}$) at the location L1 and in September (38 $mg\ l^{-1}$) at L4. The pronounced peaks of surface SPM concentration in July in L1 (50 $mg\ l^{-1}$) and in June in L4 (8 $mg\ l^{-1}$) are shaped by the advection of additional SPM mass from neighboring grid points and resuspension. The increase in the significant wave heigh at L4 in the end of June and later, in August, and September leads to the increase of the shear stress velocity and SPM concentration. This increase occurs only in the bottom layer (Fig. 5.10a)) because the additional wave mixing is not strong enough to redistribute SPM up to surface.

In the open North Sea at the location L6, the surface SPM concentrations (Fig. 5.10i) remain low throughout the simulation period ($< 0.03\ mg\ l^{-1}$) despite the erosion events and strong vertical mixing due to waves during storm periods in January-February and October-November (characterized by the wind speed of up to 20 $m\ s^{-1}$ and Hs of up to 8 m; Fig. 5.10j and k). During other months in 2002 the values of shear stress velocity in this location are generally below V^*_{res} (Fig. 5.10l) and do not cause significant increase in the SPM water concentration (annual mean SPM concentration at the surface and in the near bottom layer was 0.03 $mg\ l^{-1}$ and 0.06 $mg\ l^{-1}$ respectively). The second erosion event in October is not intensive enough to increase the SPM concentration in the bottom water layer of the model. In comparison to the first erosion event in the end of January the shear stress velocity in October is smaller (3.2 $cm\ s^{-1}$ in October and 5.6 $cm\ s^{-1}$ in January) and not high enough to erode new sediment from deeper bottom layers.

5.4 Evolution of fine sediment in the seabed

Dynamics of fine sediment in the seabed, with an exception of the exchange processes at the water-seabed interface has a different time scale from that of the

SPM processes in water. Significant changes in the fine sediment distribution compared to its initial state can occur only after a several year model simulation. However, intensive turbulence in the whole water column due to currents and waves lead to high values of the shear stress velocity in the near-bottom water layer and result in the active exchange processes at the water-seabed interface. This can somewhat change the fine sediment distribution in the seabed already on the time scale of a year. The initial fine sediment distribution in the North

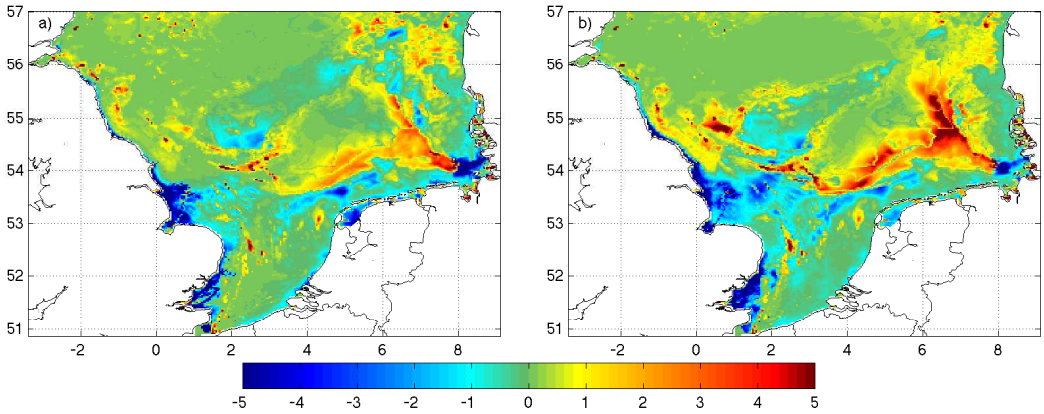

Figure 5.11: Changes in the fine sediment mass ($kg\ m^{-2}$)in the North Sea in the seabed in the end of 2002 (a) and in the end of 2003 (b) compared to initial values.

Sea (Fig. 2.3) based on the measurements and satellite data (Section 2.2.4) is used to calculate the initial fine sediment distribution in the upper 20 cm of the seabed. Evolution of fine sediment in the seabed is represented by snap-shop distributions of fine sediment mass integrated over the first 20 cm of seabed included in the model in the beginning and in the end of the simulation (Fig. 5.11). The snap-shot model results are relevant for the analysis of the long term changes in the fine sediment dynamics, because the change of fine sediment mass due to erosion and sedimentation occurs only in the upper 5-10 mm of the seabed. The mass content involved in the exchange processes between seawater and seabed is estimated based on the model simulation for the year 2002 and 2003. During this period the mean modeled erosion depth is 0.1 mm, corresponding to about 0.5 % of the total fine sediment mass in the upper 20 cm of the seabed. Therefore, the influence of instant events, such as erosion and sedimentation on the total fine sediment mass in the upper 20 cm of the seabed is not significant.

Model results show that already two years model simulation (2002 and 2003) changes the fine sediment distribution in this layer. Figure 5.11 presents this change calculated as the differences in the fine sediment mass distribution between the initial field and the modeled field in the end of 2002 (Fig. 5.11a), and in the end of 2003 (Fig. 5.11b). The range of the differences in the upper 20 cm of the seabed is between $-5\ kg\ m^{-2}$ and $5\ kg\ m^{-2}$. The negative values indicate the zones of washing-out of seabed and positive values the zones where accumulation of fine sediment in the seabed occur.

The largest differences are modeled for the zones with the highest initial fine sediment content (compare Fig. 2.3 and 5.11). The sign of the difference depends on (1) the action of the shear stress velocity, which determines the zones of washing-out, and (2) on the circulation, which transports the fine sediment from the resuspension (erosion) zones to neighboring locations. During calm conditions, SPM in these locations settles down and returns into the seabed due to sedimentation and bioturbation.

Analyses of the seasonally averaged shear stress velocity distributions (Fig. 4.3) allocate the areas in the North Sea, where the washing-out and accumulation zones of fine sediment can potentially occur. However, only analyses of the fine sediment mass change in the seabed provides specific details about these zones locations.

The main fine sediment accumulation zones are located in the German Bight stretching to the West, in the open North Sea and northwards along the coast. The zones with the negative changes in the fine sediment content (washing-out) are located mainly along the English coast, where strong current are observed. Due to additional action of the wave component of the shear stress velocity during storm events in the years 2002 and 2003, the shallow regions of the North Sea, for example the Dogger Bank, also become a washing-out zone.

Due to transport of SPM by sea currents, its settling and following sedimentation into the seabed, the zones of accumulation of fine sediment can be developed also in the deeper open North Sea locations. However, because of the general counter-clockwise circulation pattern in the North Sea (Lenhart and Pohlmann, 1997), as well as the predominated direction of storms coming mainly from the

North Atlantic, SPM is not transported to the deep regions. As a result, the content of fine sediment in these areas does not change significantly during the whole simulation period. The values of fine sediment mass difference in the deep open North Sea are close to zero, despite the high fine sediment content in the seabed (see Fig. 2.3).

5.5 Dynamics of fine sediment mass in seawater and in the seabed

Figure 5.12 presents the dynamics of SPM mass in seawater and the fine sediment mass in the seabed. The mass content in the entire model domain (Fig. 5.12b) is formed by the rivers and cliffs loads (Fig. 5.12a), net inflow through the open boundaries (Fig. 5.12c, blue line) and net seabed input (Fig. 5.12c, green line). The net inflow calculated as the difference between the mass inflow and outflow through the open boundaries shows the intensity of general circulation and exchange of SPM through these boundaries. Net seabed input is calculated as a difference between the erosion and sedimentation masses. Summary of statistical parameters of mass balance components is shown in Table 5.3.

Table 5.3: Fine sediment mass and input from rivers, cliffs, open boundaries and seabed over entire model domain in the North Sea in 2002

	min	max	mean	std
Rivers load, $kg\ s^{-1}$	92.58	446.73	189.62	79.43
Cliffs load, $kg\ s^{-1}$	140.09	1.40×10^{3}	182.37	184.37
Net inflow, $kg\ s^{-1}$	-2.38×10^{8}	1.41×10^{8}	-6.64×10^{6}	3.98×10^{7}
Net seabed input, $kg\ s^{-1}$	-4.76×10^{8}	1.56×10^{9}	-3.07×10^{5}	1.07×10^{8}
Mass in seawater, kg	1.02×10^{10}	1.51×10^{11}	5.01×10^{10}	2.28×10^{10}
Mass in seabed, kg	5.89×10^{12}	6.00×10^{12}	5.94×10^{12}	1.95×10^{10}
Total mass, kg	5.97×10^{12}	6.05×10^{12}	5.99×10^{12}	1.51×10^{10}

The total mass of fine sediment in seawater and in the seabed is a conservative value. During 2002 the mass had changed from the minimum in the end of April ($5.97\times10^{12}\ kg$) to the maximum in the end of January ($6.05\times10^{12}\ kg$) with the

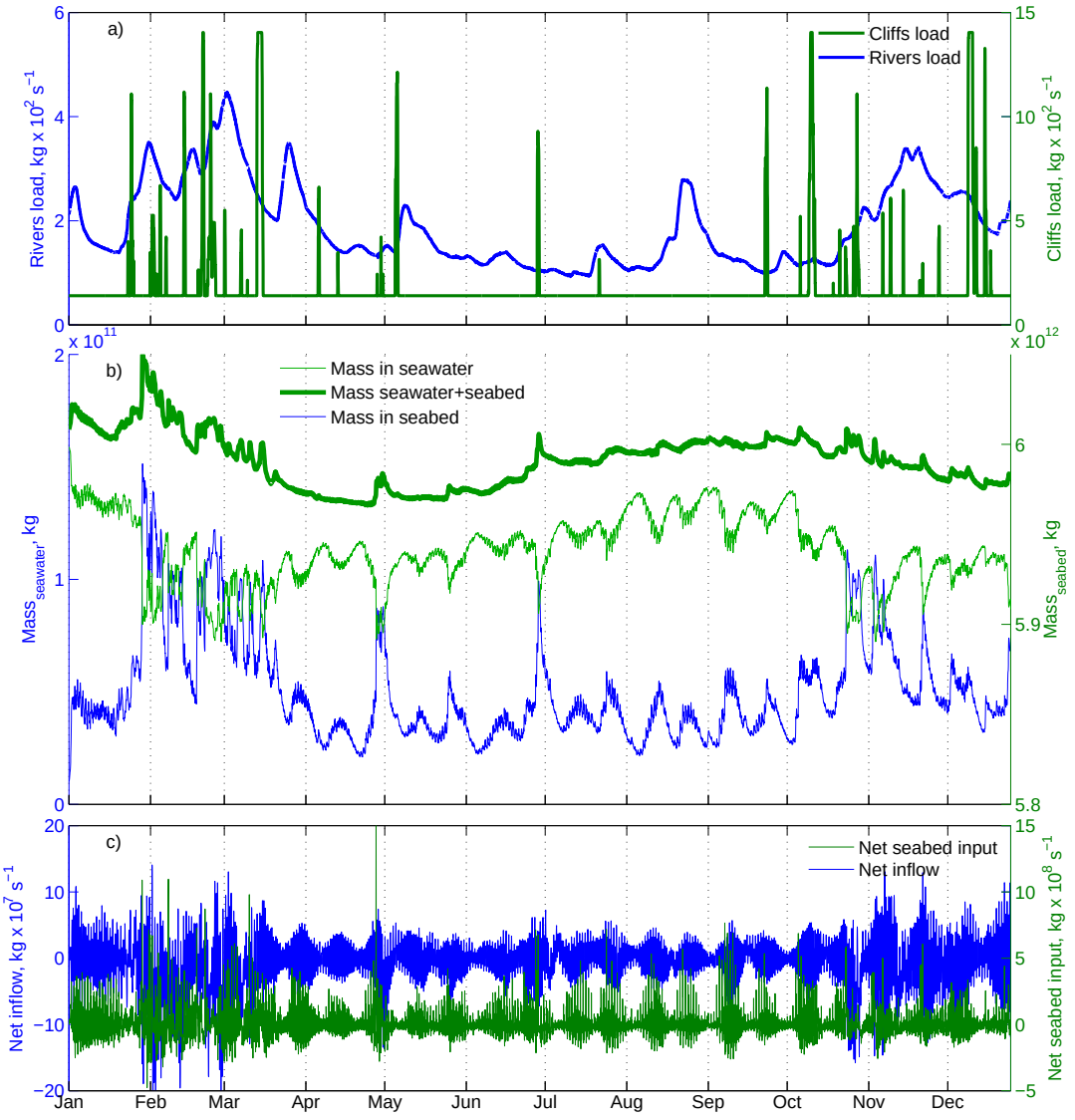

Figure 5.12: Fine sediment mass (kg) in the North Sea in 2002: a) rivers (blue line, left axis) and cliffs (green line, right axis) load b) mass in suspension in water (blue line, left axis), in the seabed (green line, right axis) and the total calculated as the sum of both (thick green line, right axis) and c) net SPM mass inflow through the open boundaries (blue line, left axis) and net seabed input (green line, right axis).

standard deviation of 1.51 $\times 10^{10}$ kg. The major changes of SPM mass in seawater are formed by the net inflow through the open boundaries in the North Atlantic and the English Channel (annual mean value -6.64$\times 10^6$ $kg\ s^{-1}$). The contribution of the rivers and cliffs loads to the SPM mass change in the modeling domain is the smallest (annual mean value 189.62-182.37$\times 10^6$ $kg\ s^{-1}$).

Fine sediment mass input from the seabed confirms the role of the seabed as a significant source of fine sediment in the North Sea. Net seabed input has the maximum in the end of April (1.56×10^9 kg, Fig. 5.12c) and forms a peak in the SPM mass in seawater, as well as in the total fine sediment mass (Fig. 5.12b). Further peaks occur later throughout the simulation period, in June, October and November of 2002. This peaks are local, because the annual mean of the net seabed input is negative (-3.07×10^5 kg). In general, the seabed is a sink of fine sediment settled from seawater. The peaks in the fine sediment mass time series are mostly caused by the SPM transport through the open boundaries and by erosion and resuspension of fine sediment from the seabed.

According to the fluxes of fine sediment mass in the entire model domain (Table 5.3), the total fine sediment mass slightly decreased during 2002, from 6.01×10^{12} kg in the beginning of the simulation to 5.98×10^{12} kg in the end of the simulation. This decrease corresponds to 0.47% of the initial mass.

Chapter 6

Results of satellite data assimilation into the CTM-SPM model

This chapter presents the results of model simulations of SPM dynamics with satellite data assimilation. Sensitivity of modeled SPM concentrations to different combinations of assimilation parameters are assessed in numerical experiments discussed in (Section 6.1). Duration of assimilation signal in the model is discussed in Section 6.2. Effect of satellite data assimilation on the modeled surface SPM distribution is evaluated in Section 6.3. Finally, Section 6.4 compares annual time series of SPM concentrations with and without satellite data assimilation.

6.1 Sensitivity of model results to assimilation parameters

In contrast to model results, satellite images provide only fragmentary incontinuous data due to technical restrictions in their processing algorithms, clouds and seabed reflection in shallow regions. With the assumption that the satellite measurements content errors, which can not be removed completely from measurements before assimilation, this study performed some model experiments with the fixed prediction error parameter σ_P in the equation 3.9 in order to study the model sensitivity on the ratio between observation error σ_O (Eq. 3.9) and σ_P.

The model sensitivity to assimilation parameters was analyzed using the statistical comparisons of model results with is-situ measurements collected during GKSS cruise in the North Sea from 23.04.2003 to 01.05.2003 (Fig. 3.2d and Table 6.2), expressed as statistical parameters (mean, standard deviation, root mean square error, correlation coefficient and bias, see Appendix 7.2) of the SPM surface concentration are summarized in Table 6.1.

In general, modeled SPM concentrations calculated with and without data assimilation have differences in the mean values (up to 0.29 $mg\ l^{-1}$), standard deviation (up to 4.77 $mg\ l^{-1}$), root mean square error (up to 4.03 $mg\ l^{-1}$) and BIAS (up to -1.32 $mg\ l^{-1}$). The correlation coefficient R is around 55% and does not change significantly in all experiments. The main effect of data assimilation is the decreasing magnitude of modeled surface SPM concentration and decreasing root mean square error. The influence of satellite data on the model results increases with the increasing of σ_O.

Table 6.1: Summary of statistic parameters calculated for the model experiments with data assimilation parameters.

σ_O/σ_P	Mean[1]	STD[2]	RMSE [3]	R[4]	BIAS
No assim.	5.39	8.68	7.90	56.2	2.38
1	5.10	3.91	3.87	54.1	2.09
2	5.15	3.94	3.90	55.3	2.14
3	5.34	4.11	4.10	55.8	2.33
5	5.96	4.77	4.92	55.6	2.95
8	6.7	5.81	6.10	56.1	3.70
Observations[5]					
-	3.00	2.33	-	-	-

[1]Mean value of surface SPM concentration
[2]Standard deviation
[3]Root mean square error
[4]Correlation coefficient
[5]GKSS cruise in the North Sea from 23.04.2003 to 01.05.2003 (Fig. 3.2d and Table 6.2)

Figure 6.1 shows the surface SPM concentrations resulted from model experiments with different observation error (σ_O) in the error observation correlation

matrix (Eq. 3.9) in comparison to in-situ measurements. The maximum of $\sigma_O = 8$

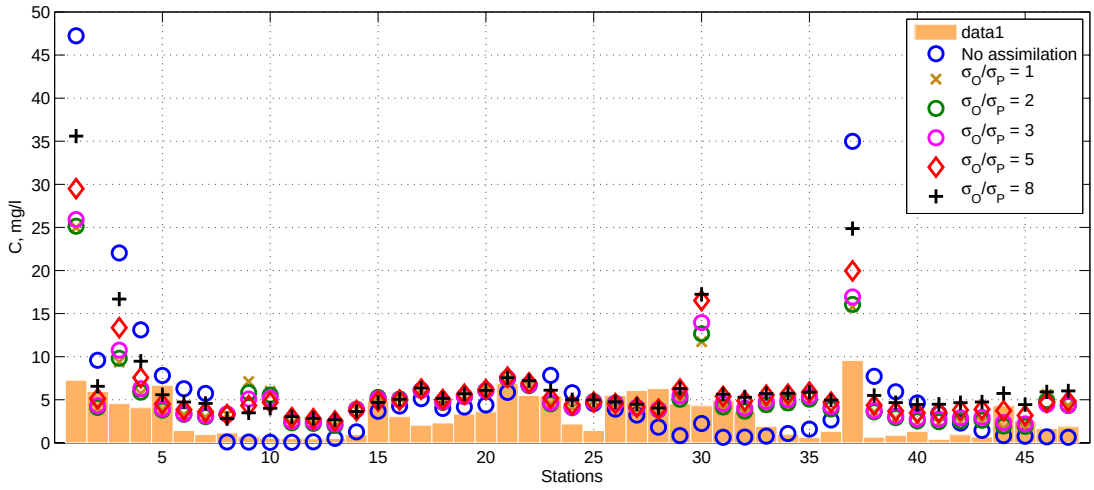

Figure 6.1: Surface SPM concentration C $(mg\ l^{-1})$ calculated by the CTM-SPM model with the variation of σ_O (different markers, see figure legend) in comparison to the model run without assimilation (blue circle) and in-situ measurements (bars) in different locations in the North Sea (stations positions showed on the figure 3.2d) in the April and May 2003

corresponds to a decrease in RMSE and STD in comparison to no-assimilation model results. But in this case, the RMSE, STD and BIAS have a maximum (5.81, 6.10 and 3.70 $mg\ l^{-1}$) in comparison to another experiments, as well as the mean value of modeled surface SPM concentration is high (5.81 $mg\ l^{-1}$) in comparison to measurements (the mean of measurements is 2.33 $mg\ l^{-1}$). The experiment with the minimum of $\sigma_O = 1$ which is equal $\sigma_P = 1$ shows the best results correspond to the minimal difference between the mean of measurements and model results (-1.58 $mg\ l^{-1}$). However, it leads to a decrease in the correlation coefficient to 54.1%. Other experiments with the σ_O = 2,3 and 5 demonstrate a decrease in the mean surface concentration, STD, RMSE and BIAS with the decreasing of σ_O. The correlation coefficient represents in this case the relationship of surface SPM distribution calculated by the model and episodic measurements. Data collected in the different parts of the North Sea were used to calculate the correlation coefficient (Fig. 3.2d). This explains the relatively low values of correlation coefficient.

The available in-situ data cover only comparatively small part of the model

simulation both in time and in space. Therefore this data set can not be representative of the whole simulation period, as well as for the entire model domain. Based on the experiments in this study, the value of σ_P was set to 1 and the value of σ_O to 2 for the main model simulation. These values were selected in order to keep the correlation coefficient close to the upper limit and smooth the effect of high SPM concentrations retrieved from satellite corresponding to the highest measured values and can contain errors.

Another satellite data assimilation parameter which was tuned in this study is the radius of influence L_{max} (m, Eq. 3.8). It is responsible for the smooth distance around each observation points and, respectively, the gradient between the first guess and assimilated fields. The effect of variations of L_{max} (Fig. 6.2) is seen in the comparison of modeled surface SPM concentration and SPM concentration obtained from the satellite. Based on the numerical experiments, the value of L_{max} was set to 6000 m (the radius of 2 grid points) in order to include in the model the fine horizontal structure obtained from satellite.

6.2 Duration of assimilation signal in the model

To evaluate the duration of the assimilation signal in the model the *one assimilation event* experiment was performed. In this experiment, the model was run with only one assimilation event on the 22 March 2003 at 10:12. The test model simulation started on 1 January 2003 without data assimilation. When the model reached 22 March 2003, the MERIS data were assimilated into the simulation continued until 30 April 2003 without further data assimilation. The spatial coverage by satellite measurements in this assimilated scene was about 40% of the model area. The results of this experiment are shown in the time series of mean surface SPM concentrations over the whole model area with and without data assimilation (Fig. 6.3b). The forcing is represented by wind speed and significant wave height averaged over the model domain (Fig. 6.3a). Behavior of mean surface SPM concentration during this experiment follows the changes in forcing. Maximum of mean wind speed (16.2 $m\ s^{-1}$) and significant wave height (5.1 m) located between the 10th and the 12th day of the simulation (Fig. 6.3a) is presented on the

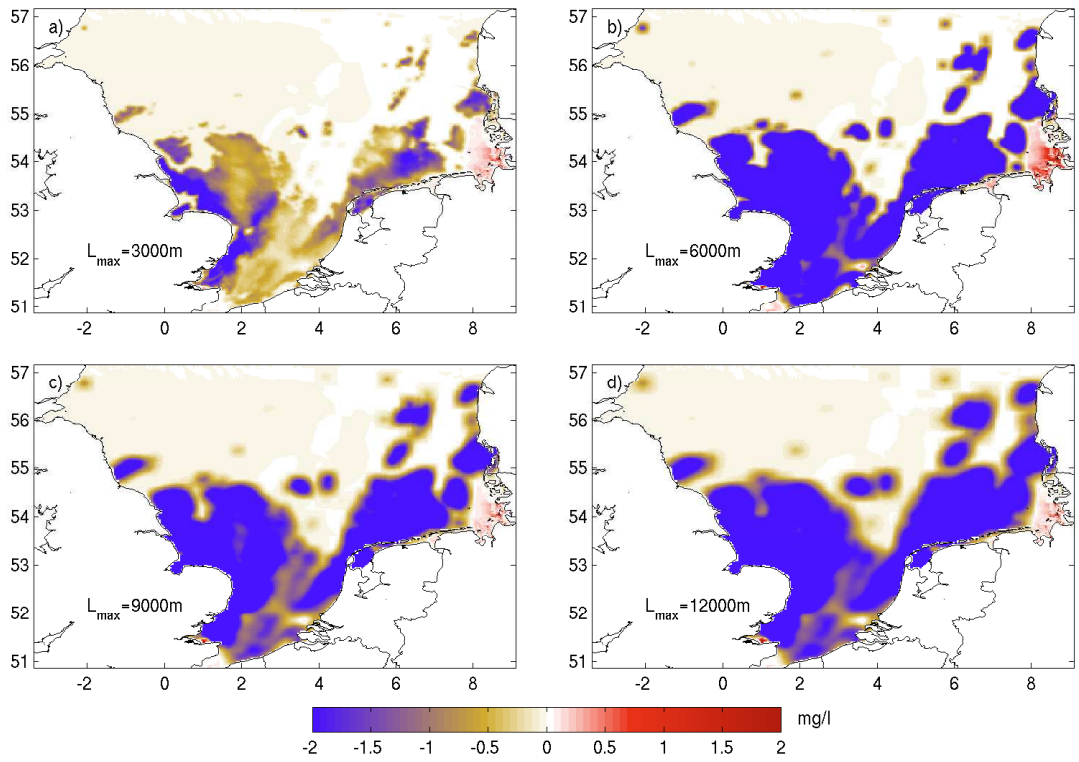

Figure 6.2: Differences of the surface modeled SPM concentration ($mg\ l^{-1}$) before and after data assimilation with different radius of influence L_{max} (m).

mean SPM time series later, on the 16th to 18th day of the simulation (Fig. 6.3b). According to the North Sea topography (Fig. 2.3), the highest waves coming from the North Atlantic are expected in the deep open part of the model domain (Fig. 4.2). The changes of surface SPM concentration in these areas during storm are insignificant. The storms wave height decreases while it propagates to the shallow coastal areas, but it is still hight enough to cause strong vertical mixing in the shallow areas and leads to an increase in the surface mean SPM concentration from 2-3 $mg\ l^{-1}$ to 6-7.5 $mg\ l^{-1}$. This explains the time lag of a few days between the peaks in the forcing date and the modeled local surface SPM concentration. The difference between the modeled mean surface SPM concentration with and without satellite data assimilation calculated from this experiment has the peak directly after the assimilation event (22 March 2003 10:00). Its magnitude decreases quickly by 50% in the first 3 days after the assimilation event. The SPM mean surface concentration after OI-assimilation increases and reaches 3.9 $mg\ l^{-1}$. The maximum difference in the concentrations with and without assimilation is

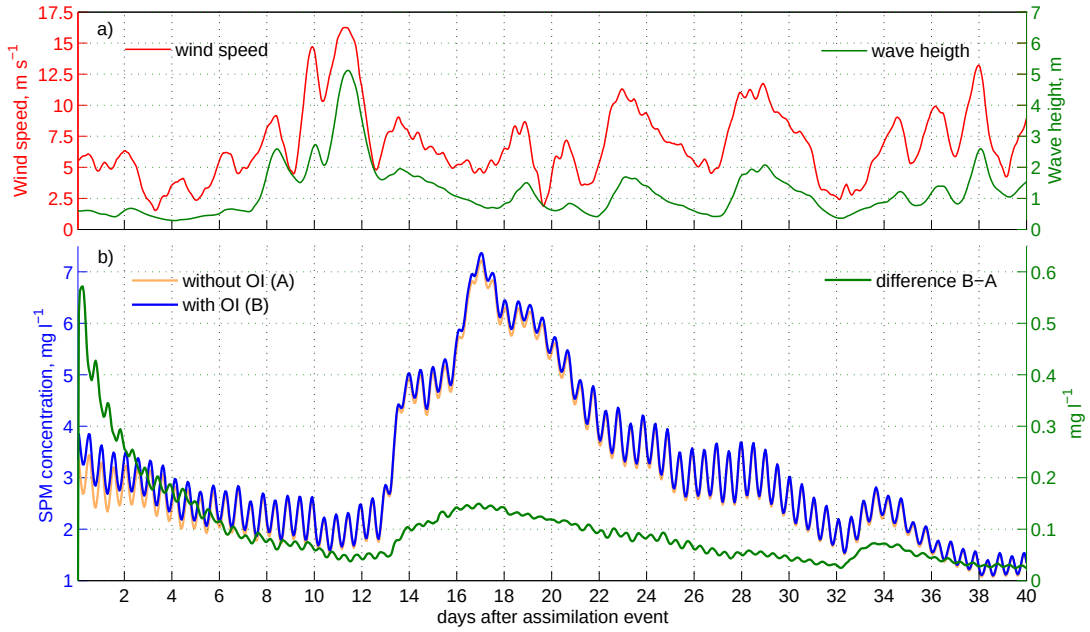

Figure 6.3: Duration of assimilation signal after the OI event on 22 March 2003 at 10:12: a) wind speed averaged over the model domain (red line, left axis) and wave height (green line, right axis); b) mean surface SPM concentration $mg\ l^{-1}$ on the without assimilation (orange line, left axis), with assimilation (blue line, left axis) and the difference between them (green line, right axis).

0.58 $mg\ l^{-1}$). Direct signal of assimilation is still present in the model after several days (6-8 in this case). During this period, additional SPM mass sinks down and reaches the seabed. Depending on the current and wave conditions, SPM starts to sediment or re-suspend. Afterward, under calm conditions that followed this period, the both mean surface SPM concentrations decrease and are located in the low SPM concentration zone (2-3 $mg\ l^{-1}$).

The peak of mean surface SPM concentration in two weeks after the assimilation event illustrates an increase of turbulent mixing in the water column due to the currents and waves. As described in Section 3.1, the assimilation in the upper water layer of the model leads to the correction of the fine sediment mass in whole water-seabed system. Therefore, even after 17 days following the assimilation event, the additional SPM mass assimilated in the model can be resuspended under storm conditions leading to the increase of the difference in the SPM concentrations between model results with and without satellite data assimilation (second peak 0.15 $mg\ l^{-1}$).

6.3 Effect of satellite data assimilation on the modeled surface SPM distribution

Two subsequent MERIS scenes on 30.03.2003 and 03.04.2003 illustrate the impact of data assimilation on the surface SPM concentration (Fig. 6.4a and b). The small significant wave heights ($Hs \approx 0.5m$, at k13, Fig. 6.4i) indicate calm weather conditions the southern part of North Sea between 29 and 30 March. Starting from 31 March Hs increases and has a maximum of 3.0 m between 2 and 4 April. Two MERIS scenes clearly reproduce such sea surface state. The first one (Fig. 6.4a) shows an SPM plum generated by cliffs and seabed erosion and propagating from English cliffs to the open North Sea in accordance with the mean counter-clockwise general circulation pattern. The second scene (Fig. 6.4b) reproduces an increase of seabed erosion, cliffs washout and vertical mixing due to waves resulting in the higher surface SPM concentration in the open North Sea (near the Dogger Bank from about 5 to 10 $mg\ l^{-1}$). Generally, the model in no assimilation mode underestimates the surface SPM concentration near English cliffs and in the open North Sea (Fig. 6.4g and h). Due to assimilation of MERIS data more details of SPM surface distribution is captured (Fig. 6.4e and f). Note that, the signal of assimilation is still present in the model 4 days after the assimilation event. The results of the first assimilation event Fig. 6.4e is still present in the next first guess field Fig. 6.4d.

Figure 6.5 shows two seasonal means of SPM surface concentrations for the calm period (15 April - 15 October 2003; Fig. 6.5a and c) and for the storm period (15 October - 15 April 2003; Fig. 6.5b and d) modeled with and without assimilation respectively. The comparison between these two model simulations show that the effect of assimilation remains in the model on a long time scale (1 year). Especially for the calm period and for SPM concentrations $< 10\ mg\ l^{-1}$, the effect of assimilation is more pronounced (cf. Fig 6.5a and c). The whole horizontal SPM distribution structure from English cliffs to the German Bight and the SPM front in the German Bight changed due to assimilation. For the storm period and SPM concentrations $> 10\ mg\ l^{-1}$ the effect of assimilation on the structure of the horizontal distribution of SPM is weaker. The change due to assimilation is more related to the magnitude of SPM concentration (cf. Fig.

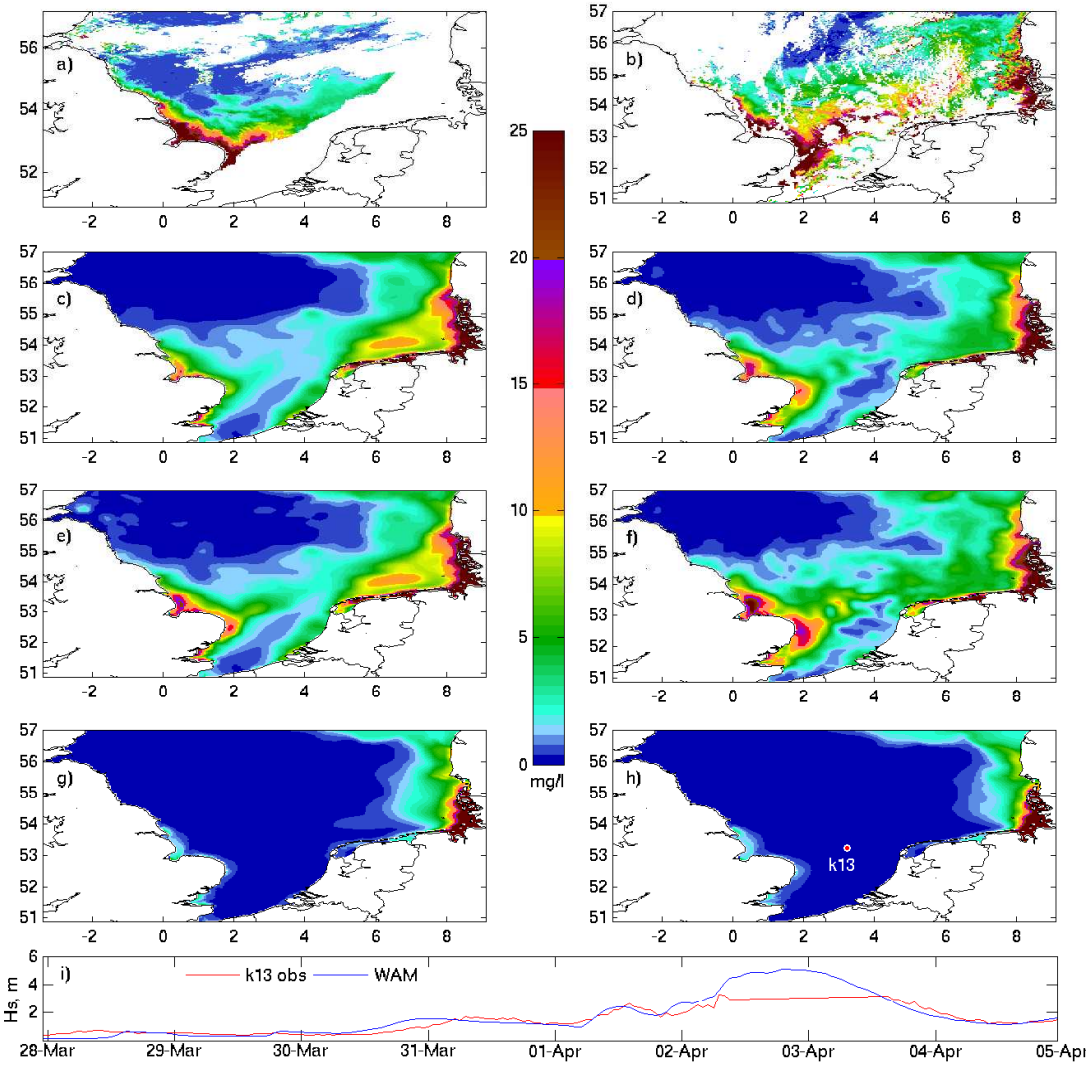

Figure 6.4: SPM surface concentrations on 30.03.2003 at 11:00 and on 03.04.2003 at 10:43 calculated from MERIS data (a and b); calculated by the model before assimilation (first guess, c and d); calculated by the model with OI assimilation (e and f); calculated by the model without data assimilation (g and h); modeled (i, blue) and observed (i, red) significant wave height in location K13 (shown on the map).

6.5b and d). Figure 6.6 shows a comparison of model results with observational data collected during GKSS cruise in the North Sea from 23.04.2003 to 01.05.2003 (Fig. 3.2d and Table 6.2).

For individual measurements, the effect of data assimilation is more pronounced for high SPM concentrations ($> 20\ mg\ l^{-1}$). Compared to the no assimilation run, satellite data assimilation clearly improved overestimated modeled

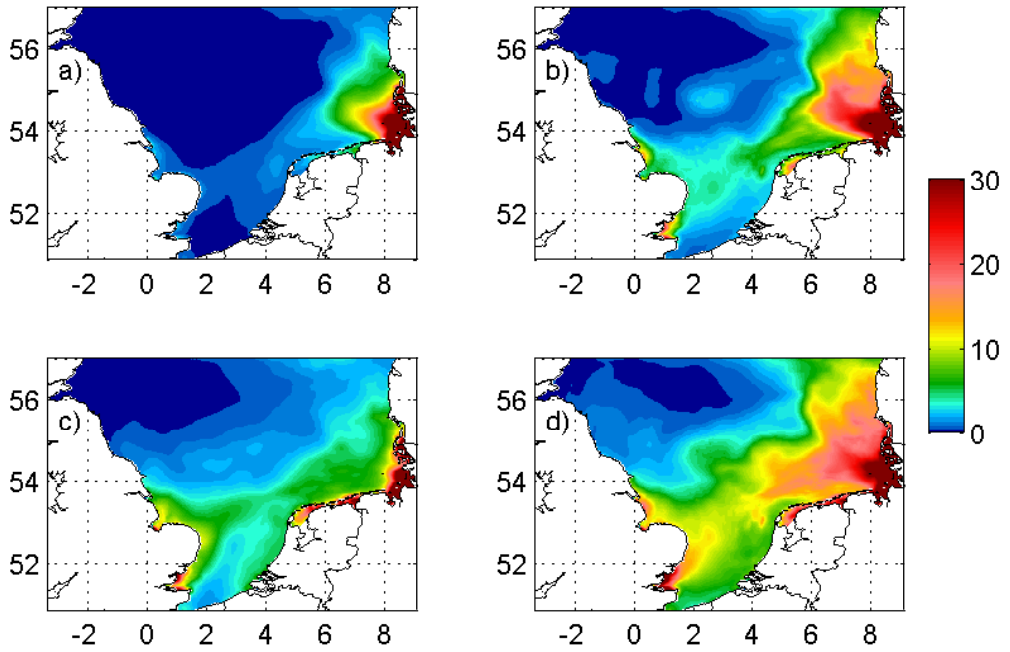

Figure 6.5: Seasonal mean SPM surface concentration ($mg\ l^{-1}$) calculated by the model in the year 2003 for the calm (15 April - 15 October) and storm (15 October - 15 April) seasons without assimilation (a and b), with assimilation (c and d).

concentrations in locations 1, 2, 3 and 37 (Fig. 6.6). For all analyzed observational locations, the assimilation decreases the difference between observation and model results (BIAS is 2.38 $mg\ l^{-1}$ for the model without assimilation and 2.09 $mg\ l^{-1}$ with assimilation).

Table 6.2: Overview of SPM in-situ data for the year 2003 used for the evaluation of model results (range and mean of measured and modeled SPM concentrations).

Observations, $mg\ l^{-1}$		Model with assimilation, $mg\ l^{-1}$		Model without assimilation, $mg\ l^{-1}$	
range	mean	range	mean	range	mean
0.41-9.56	3.00	1.67-24.99	5.10	0.07-47.23	5.39

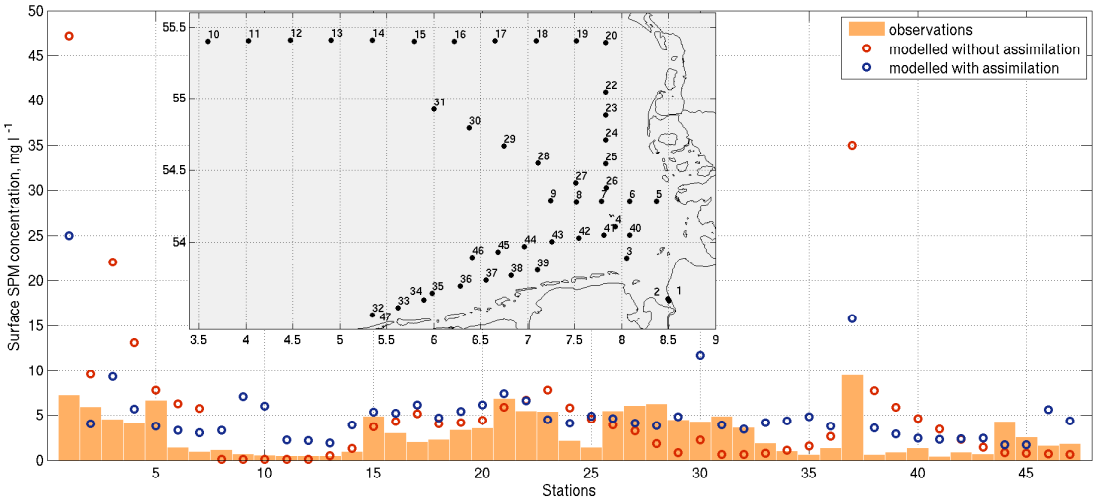

Figure 6.6: Surface SPM concentration ($mg\ l^{-1}$) in various stations observed and modeled with and without assimilation. Geographical location of stations is shown on the map.

6.4 Annual time series of SPM concentrations with and without assimilation

Six locations in the different parts of the North Sea (Fig. 2.3) were selected in order to analyze the temporal evolution of SPM. Table 6.3 shows the overview of effect of data assimilation in these locations. Generally, for all locations (excepting $L1$ in near-bottom layer) the effect of satellite data assimilation leads to decreasing of modeled SPM concentration in the surface, as well as in the near-bottom layers (see Table 6.3, A-B section has negative values). The mean differences between modeled SPM concentration with assimilation and without are:

- for the mean SPM concentration -0.6 $mg\ l^{-1}$ in surface and -9.5 $mg\ l^{-1}$ in the near-bottom layer
- for the minimum of SPM concentration -0.1 $mg\ l^{-1}$ in surface and -0.5 $mg\ l^{-1}$ in the near-bottom layer
- for the maximum of SPM concentration -16.0 $mg\ l^{-1}$ in surface and -39.0 $mg\ l^{-1}$ in the near-bottom layer

Table 6.3: Modeled SPM concentration ($mg\ l^{-1}$) in the locations $L1$-$L6$ A - with data assimilation, B - without data assimilation and A-B - the difference in the surface and near-bottom layers.

		Surface						Near-bottom layer					
		L1	L2	L3	L4	L5	L6	L1	L2	L3	L4	L5	L6
A	mean	31.8	0.2	1.8	3.9	0.7	0.2	117.1	7.7	45.9	17.6	19.4	0.9
	min	2.1	0.0	0.1	0.0	0.0	0.0	21.8	0.2	6.4	2.2	0.7	0.0
	max	161.9	4.1	10.3	27.9	5.6	8.1	247.6	28.5	104.2	79.5	80.2	22.9
B	mean	32.8	0.3	3.7	4.0	1.0	0.4	114.8	15.1	84.3	23.5	26.2	1.5
	min	2.9	0.0	0.1	0.0	0.0	0.0	15.8	0.3	13.9	3.3	1.1	0.0
	max	208.1	4.2	26.0	46.3	9.9	19.5	247.3	66.8	226.9	88.8	117.6	49.5
A-B	mean	-1.0	-0.1	-1.9	-0.1	-0.3	-0.2	2.3	-7.4	-38.4	-5.9	-6.8	-0.6
	min	-0.8	0.0	0.0	0.0	0.0	0.0	6.0	-0.1	-7.4	-1.1	-0.4	0.0
	max	-46.2	-0.1	-15.7	-18.4	-4.3	-11.4	0.3	-38.3	-122.6	-9.3	-37.4	-26.6

The effect of satellite data assimilation in the location $L1$ in the German Bight (Fig. 6.7a) is low in the surface and in the near-bottom layers (annual mean surface SPM concentration with data assimilation is 31.8 $mg\ l^{-1}$, without 32.8 $mg\ l^{-1}$) because currents and waves in this area with the depth of 39 m lead to the permanently strong vertical mixing during the whole year, which is well captured by the model.

Time series in the deep (61 m) location $L2$ in the western part of the North Sea (Fig. 6.7b) shows the influence of data assimilation on the SPM concentration in the near-bottom water layer. Due to correction of SPM concentration profile in the water column after assimilation in the surface layer, the mean annual SPM concentration in the near-bottom water layer changes from 15.1 $mg\ l^{-1}$ (without assimilation) to 7.7 $mg\ l^{-1}$ (with assimilation). The difference between SPM concentration with and without assimilation decreases throughout the year, particularly in the period between April and October, from $30 - 40 mg\ l^{-1}$ in April down to $3 - 5\ mg\ l^{-1}$ in August. Later in the year, with the beginning of storm period and decreasing of the number of data assimilation events, this difference grows up to 20 $mg\ l^{-1}$.

As was shown in Section 6.3, the model in the no-assimilation mode underestimates the role of the English Cliffs as one of the main sources of SPM in the southern part of the model area. The time series of SPM concentration in the

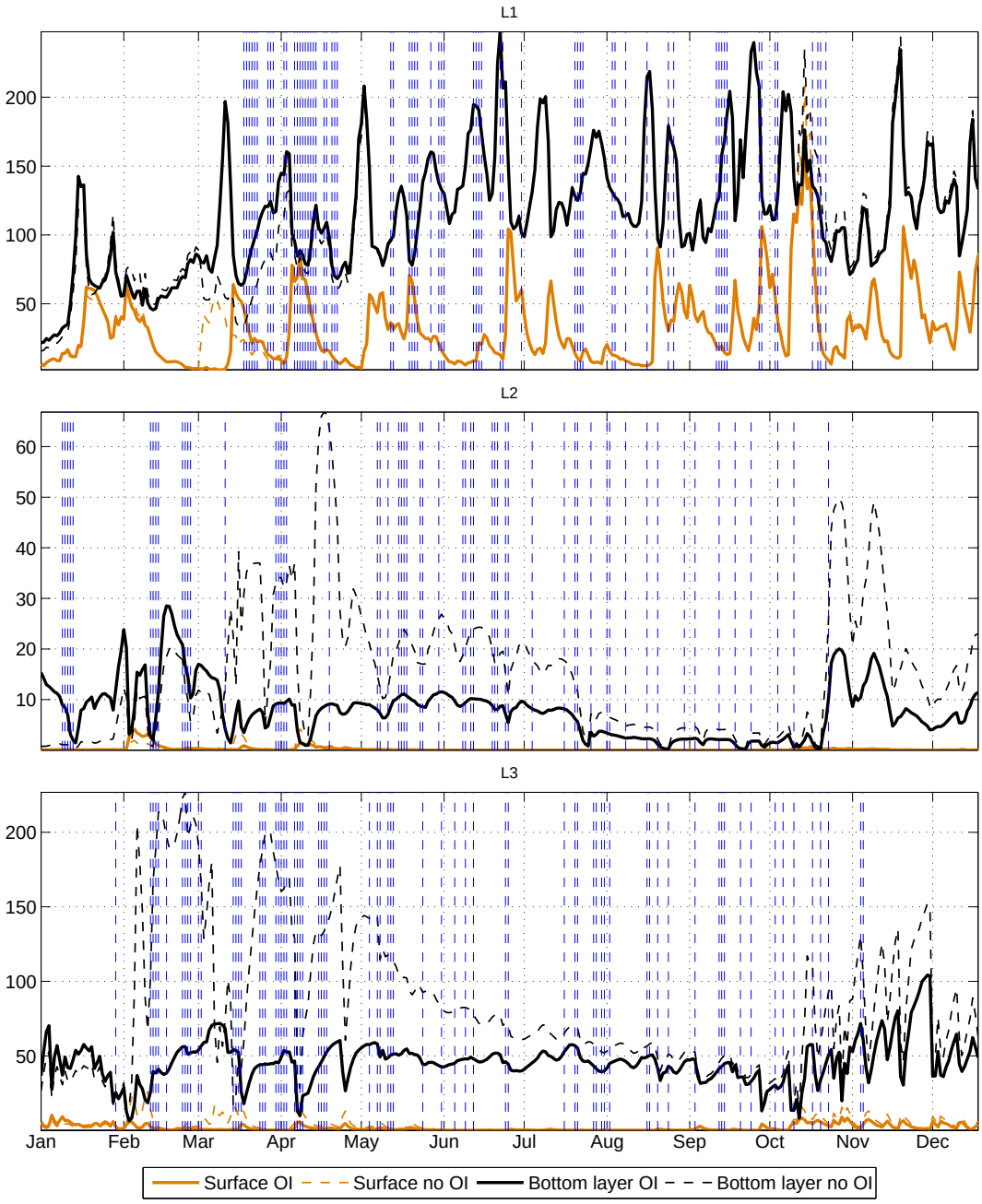

Figure 6.7: Calculated time series of daily SPM concentrations ($mg\ l^{-1}$) in the North Sea in 2003 at locations a) L1, b) L2 and c) L3 in the surface layer (orange line) and in the near bottom water layer (black line) with data assimilation (solid line) and without (dash line). The vertical dash lines show the data assimilation events.

location $L3$ near the English Cliffs (Fig. 6.7c) illustrates the significant effect of data assimilation at the surface and in the near-bottom layer (see Table 6.3). The

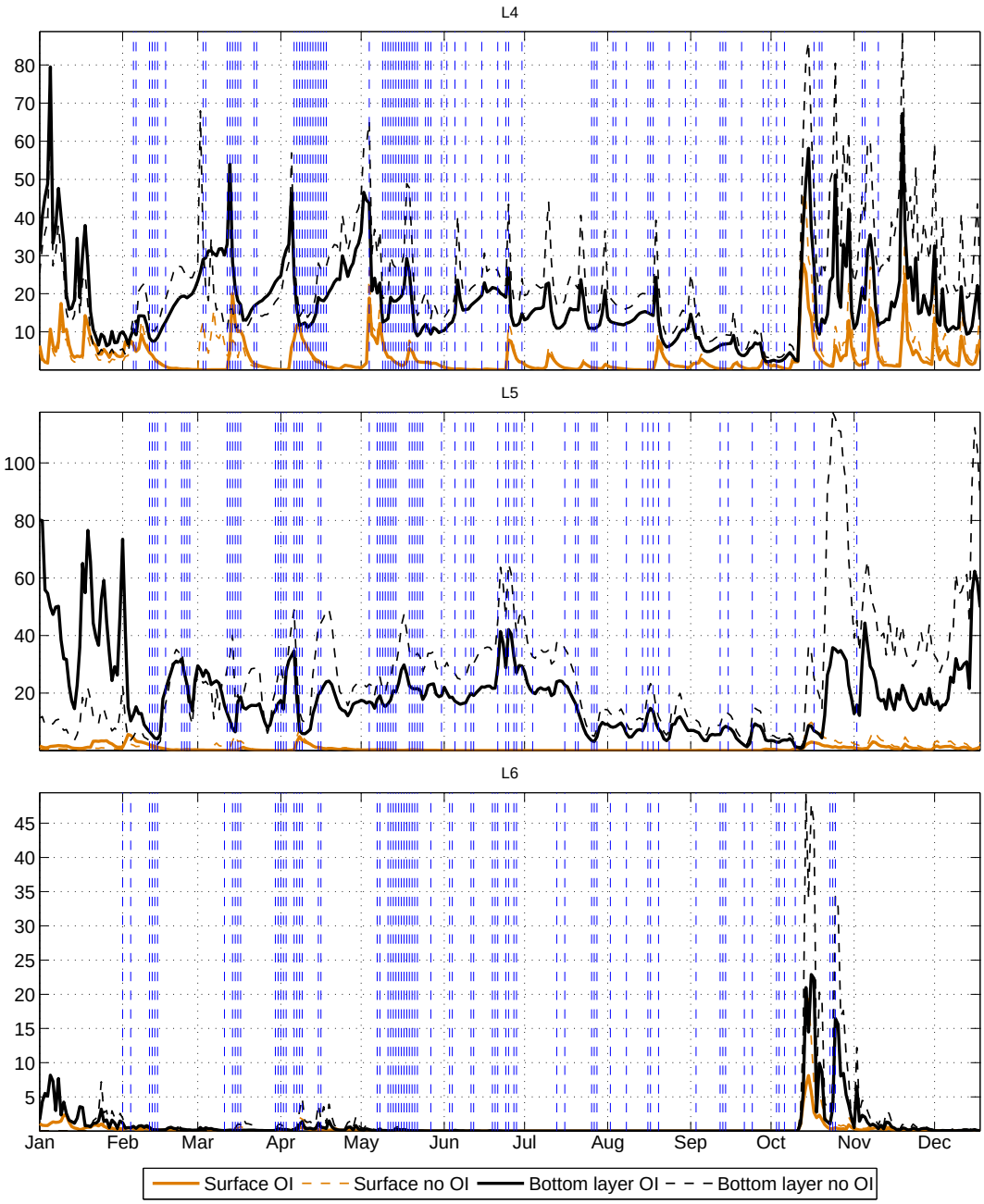

Figure 6.8: Calculated time series of daily SPM concentrations ($mg\ l^{-1}$) in the North Sea in 2003 at locations a) L3, b) L4 and c) L6 in the surface layer (orange line) and in the near bottom water layer (black line) with data assimilation (solid line) and without (dash line).

difference between daily modeled SPM concentrations with and without assimilation in the February and March in this location in the bottom layer is up to 150

$mg\ l^{-1}$ and up to 15 $mg\ l^{-1}$ at the sea surface. It decreases later in the year in August-October down to 5 $mg\ l^{-1}$ in bottom layer and 0 $mg\ l^{-1}$ at the surface due to the more frequent assimilation events before the beginning of the storm period.

The location $L4$ (Fig. 6.8a) has the minimum of fine sediment content in the bottom compared to the other locations ($L1 - L6$, see Table 5.2). However, the influence of currents on the SPM concentration is significant here. They transport SPM from the English Cliffs and from the River Rhine. The model reproduces this circulation patterns well, therefore the effect of data assimilation is not very strong. In comparison to the model results with assimilation, the difference of mean annual SPM concentration (calculated from daily values) without data assimilation is only $-0.1\ mg\ l^{-1}$ in the surface layer and $-5.9\ mg\ l^{-1}$ in the near-bottom layer.

In the deep (60 m) location $L5$ near the Dogger Bank (Fig. 6.8b), surface SPM concentration does not change significantly during the year. The shear stress velocity and vertical mixing due to currents and waves in this deep location are not strong enough to redistribute SPM from the near-bottom layer to the surface (see Table 6.3 A-B surface section).

Finally, in the open North Sea, in location $L6$ (Fig. 6.8c), where the SPM concentration is low in the whole water column (annual mean SPM concentration without assimilation at the surface is 0.2 $mg\ l^{-1}$ and 0.9 $mg\ l^{-1}$ in the near-bottom layer), the effect of data assimilation is visible only during the storm period.

Chapter 7

Concluding discussion

This chapter draws conclusions of the thesis. The key results from each chapter are summarized in Section 7.1. Section 7.2 discusses the limitations of this study and gives an outlook for future work.

7.1 Summary of key results

Suspended Particulate Matter (SPM) influences the light penetration depth in seawater and thus is an important constituent of marine ecosystems, i.e. the North Sea, where SPM concentrations are relatively high. Fragments of SPM dynamics are captured from space. The motivation of this study was, therefore, to develop a method combining modeling and satellite data assimilation for continuos calculations of SPM dynamics in the North Sea, which can be used for operational purposes and in ecosystem modeling (Chapter 1).

Chapter 2 describes the three-dimensional Circulation and Transport Model for Suspended Particulate Matter (CTM-SPM). This model is based on the existing, improved and newly designed routines for continues calculations of the long-term circulation, waves and SPM dynamics. The model includes major processes governing the dynamics of SPM, such as transport with ocean flow, exchange processes at the water seabed interface (i.e. SPM sedimentation, resuspension and erosion), as well as processes in the water column and in the seabed. SPM sources in the seabed, rivers and the cliffs combined with the meteorological and

wave forcing constrain the model processes within the southern North Sea. The model simulation period covered the years 2002 and 2003.

Chapter 3 presents a newly developed concept of assimilation of the surface SPM concentration retrieved from the satellite snap-shot images (i.e. MERIS) into the CTM-SPM using the sequential Optimum Interpolation (OI) scheme.

Quality control system based on the model results and on flags information calculated by the MERIS Case-2 Regional Processor was designed. This control system filters out unrealistic values of the SPM surface concentration and can be used for operational purposes. In this study, more that 300 MERIS scenes were assimilated into the SPM model throughout the year 2003.

One of the two major questions addressed in this study was the relative impact of currents and waves on the horizontal and vertical distributions of SPM in the North Sea and its seasonality. Chapter 4 presents the dynamics of currents and waves as the two major forcing factors in the SPM dynamics. They influence the turbulence intensity and vertical mixing in the water column, as well as the shear stress in the near-seabed water layer, which drives the seabed-water exchange processes of SPM. Analysis of the forcing factors dynamics indicates that:

- The clear seasonality of the shear stress velocity during the calm (April - October) and storm period (October - April) is attributed to the increasing turbulence intensity during the storm period due to currents and waves, especially in the shallow region of the North Sea (e.g. the Dogger Bank). The wave-induced component of the shear stress velocity dominates in the shallow regions during the entire storm period (see Chapter 4).

- The seasonal mean shear stress velocity distribution allows to classify the southern North Sea in terms of different zones where one or another seabed water exchange process dominate. The sedimentation zone is located mainly in the open North Sea, the zones of resuspension occupy the shallow regions along the coast and the open North Sea around the Dogger Bank. The zones where erosion occurs are located in the English Channel, along the UK east coast and in the German Bight. Individually or acting in concert, both currents and waves potentially lead to erosion in this areas of the North Sea

(see Section 4.3).

In Chapter 5 the model is applied to map the SPM distribution in the North Sea in the years 2002 and 2003. The model was able to reproduce the specific dynamics of SPM in the North Sea SPM capturing the stepwise character of SPM processes. Modeled SPM concentrations in seawater, as well as SPM mass and fine sediment content in the seabed are analyzed in details. SPM horizontal and vertical distributions are in good agreement with availible in-situ measurements and satellite observations. The key results of this chapter indicate that:

- Modeled SPM dynamics reveal two different patterns in the SPM dynamics in the North Sea. One is observed under calm conditions, common for the summer period. SPM distribution then is mainly shaped by the horizontal currents, which determine the location of the SPM front. Another pattern evolves instantly during storms and in the course of stormy periods. The vertical mixing due to waves dominates all other transport process and determines the vertical SPM concentration profile. The highest surface SPM concentrations were reproduced in the storm period reaching 120 $mg\ l^{-1}$ in the open North Sea and up to 300 $mg\ l^{-1}$ near the coast in the German Bight (see Section 5.1).

- In the shallow regions close to the coast and river mouths, the SPM front occurs due to resuspension, erosion and vertical mixing. Fluvial SPM does not contribute much to this because it sinks relatively fast and deposits close to the rivers estuaries (see Section 5.1).

- Intensive turbulence in the whole water column due to currents and waves lead to high values of the shear stress velocity in the near-bottom water layer and result in the active exchange processes at the water-seabed interface. This can somewhat change the fine sediment distribution in the seabed already on the time scale of a year. Model results show that a relatively short two years model simulation in the period between 2002 and 2003 can already capture changes of the fine sediment distribution in the seabed. It allows to define areas in the North Sea, where the washing-out and accumulation zones of fine sediment can potentially occur. These zones correspond to

the location of sedimentation, resuspension and erosion zones which were determined by the analyses of the seasonally averaged shear stress velocity distributions (see Chapter 4).

- The main fine sediment accumulation zones are located in the German Bight stretching westwards, in the open North Sea and northwards along the coast. The washing-out zones are located mainly along the British coast, where strong currents are observed. Due to additional action of waves, the shallow regions of the North Sea, for example the Dogger Bank, may also become a washing-out zone (see Section 5.4).

- Oscillations in the SPM mass in seawater mirror the bottom fine sediment mass dynamics. The sum of both shows the changes of the SPM concentration and the fine sediment mass in the water-seabed system and their seasonal variations. The total fine sediment mass in suspension and in the first 20 cm of the seabed is about 6×10^{12} kg. Relative mass oscillations throughout the year are around 1.5% (see Section 5.5).

- Model results suggest that it is essential to use a coupled circulation and SPM transport model with a realistic forcing data with a temporal resolution of < 1 hour and instant values of shear stress velocity in order to resolve the SPM processes of different time scales, e.g. flash erosion events and long-term transport by currents. Utilization of the instant values of the shear stress velocity leads to more realistic representation of the exchange processes at the water-seabed interface and to more convenient comparison between the snap-shot satellite measurements and model results (see Sections 5.3 and 5.1.2).

Another major question that was addressed in this study (see Section 1.2) was the feasibility of assimilation of the currently available satellite data into an SPM transport model and the effect of data assimilation on the model results. Satellite data are restricted by a number of shortcomings, such as constraints in the processing algorithms, clouds or seabed reflection in shallow regions. Chapter 6 presents the first attempt of continual satellite data assimilation into an SPM

transport model. The results of this attempt indicate a great potential for the application of satellite optical data in the SPM modeling.

- After processing and quality control, surface SPM concentration obtained from the satellite data can be assimilated into the uppermost layer of the model (see Chapter 6).
- Assimilation effects not only the SPM concentrations in the surface, but also penetrate into the whole water column, and even effect the fine sediment distribution in the seabed (see Section 6.4).
- The data assimilation signal remains in the model for several days after assimilation, which is long enough for the next assimilation event (see Section 6.2).
- Satellite data assimilation improves the horizontal SPM distribution, especially its fine structures in the locations of SPM front in the German Bight and near the English cliffs (see Section 6.3).
- The seasonal distribution patterns of SPM changed considerably due to assimilation (see Section 6.3).

Based on the modeling alone or combined with the satellite data assimilation, the concept presented in this study can be used for continuous long-term calculations of SPM dynamics in the North Sea. Although it has some restrictions discussed in Section 7.2, it can serve as the basis for operational purposes and in ecosystem modeling.

7.2 Limitations and thoughts for future work

SPM concentrations at the sea surface that can be observed by satellites descend from the interaction of processes in the whole water column and the fine sediment exchange processes at the seabed-water interface. Moreover, results presented in Chapter 5 showed that the dynamics of SPM in the whole water column depends on the current weather and sea state conditions. Particularly, strong wind and

waves enhance vertical mixing leading to an increase of shear stress at the seabed. Therefore, modeling of SPM has to include the processes in different environmental compartments, such as the atmosphere (wind stress), seawater (currents, waves and turbulent mixing) and seabed (fine sediment distribution as the major source of SPM in the North Sea). This thesis reports on the SPM dynamics in the North Sea calculated using an assemblage of various models. Presented model results show that such approach of SPM modeling is sufficient to represent and understand the SPM dynamics and processes occurring in nature.

Furthermore, SPM processes, e.g. erosion and resuspension are stepwise and instant. This study shows that they are better captured using fine temporal resolution. Averaging of forcing data in time smoothes the intensity of fine sediment mass exchange between the seabed and water. Therefore, it is important to calculate all forcing parameters for SPM on the same temporal scale.

The most significant gaps to be filled for future development and application of the models of SPM dynamics are as follows:

- *Refined modeling tools.*

  First, higher spatial resolution is needed to improve the results of an SPM model on the scale of the North Sea. Fine spatial resolution is particularly critical in the deeper water layers, close to the seabed. It would enable more realistic simulations of the fine sediment mass exchange between seabed and seawater and its redistribution in the whole water column.

  Second, current model setup uses Z-coordinate system. Some shallow areas with an average depth of 5 meters are represented by only one layer in the model. If this is the case, all model processes occur in this layer. Such approach smoothes the contribution of each individual process and does not allow to capture the details of SPM dynamics in the shallow model area. Following the general circulation in the North Sea, the redistribution of SPM from shallow and coastal regions to the open North Sea is one of the main factors responsible for the location of SPM fronts. A sigma-coordinate system with the model layers following the topography and irregular model grid (finer in the coastal areas and coarser offshore) would resolve the small-

scale processes in the very shallow coastal regions in details.

- *Improved processes parameterization.*

  Local factors, such as SPM contribution from the rivers and cliffs play significant role in the small-scale SPM dynamics in coastal areas. The model results obtained without the satellite data assimilation, compared against the run with assimilation (see Chapter 6) show that the model in no assimilation mode is not able to reconstruct the SPM structure near the English Cliffs, which is visible from satellite. Therefore, more realistic parameterization of the erosion from cliffs is needed.

  Flocculation (the process whereby the particles of fine sediment conglomerate leading to formation of larger-size flocs) of SPM can also play an important role in its dynamics in the North Sea. Especially in the high SPM concentration zones, where calm conditions prevail, for example in the near-bottom layers in the deep part of the North Sea (see Section 5.2). Flocculation process increases the grain size and sinking velocity of suspended material and can result in the change of the intensity of gravitational settling. This in turn, will have an impact on the exchange processes at the water-seabed interface (i.e. sedimentation and resuspension). Although, flocculation is not included in the current model setup, it can be included in the model as additional fractions of SPM, which are steered by the shear stress velocity like other SPM fractions, but additionally have a turbulence-induced aggregation and floc break-up. This processes can be derived, for example, from a recent study presenting an analytical solution of a Lagrangean flocculation model (Winterwerp et al., 2006).

- *Amendments to initial data.*

  Finally, the role of seabed as the main source SPM in the North Sea can be better reproduced using more complicated methods (in comparison to method described in the Section 2.1.5) for the simulation of bio-activity in the seabed in the North Sea.

The results of this study indicate that satellite data assimilation improves the fine horizontal structure of SPM at the sea surface and corrects the SPM

mass content in the whole water column (Chapter 6). Therefore assimilation of SPM concentrations retrieved from MERIS can potentially improve not only the surface model layer concentration, but also the vertical profile of SPM and the seabed distribution of fine sediment.

However, ocean color data does not directly provide the vertical distribution of measured parameters in seawater. A method is needed, which can be used to reconstruct the vertical profile of SPM in the water column for the satellite measurements. Furthermore, the flags technique to allocate the invalid pixels in the satellite data processing (Section 3.3) need to be improved in order to use more realistic measurements for the data assimilation purposes.

Appendix: Statistical parameters used for results analyses

By the analysis of model results and by comparison with the in-situ and satellite measurements the following statistical parameters are used.

Mean values of the model results and measurements were calculated by:

$$\bar{x} = \frac{1}{n} \sum_{i=1}^{n} x_i \tag{7.1}$$

The standard deviations of model results and measurements were defined as:

$$\sigma_x = \sqrt{\frac{1}{n-1} \sum_{i=1}^{n} (\bar{x} - x_i)^2} \tag{7.2}$$

The root mean square error for the measurements x and model results y given by:

$$RMSE = \sqrt{\frac{1}{N_{obs}} \sum_{i=1}^{N_{obs}} (x_i - y_i)^2} \tag{7.3}$$

The bias was calculated for the measurements x and model results y by:

$$BIAS = \frac{1}{N_{obs}} \sum_{i=1}^{N_{obs}} y_i - x_i \tag{7.4}$$

The correlation coefficient between model results y and measurements x given by:

$$R = \frac{\sum_{i=1}^{n} (x_i - \bar{x}) (y_i - \bar{y})}{\sqrt{\sum_{i=1}^{n} (x_i - \bar{x})^2 \sum_{i=1}^{n} (y_i - \bar{y})^2}} \tag{7.5}$$

Nomenclature

SPM	Modeled suspended matter	-
ISM	Inorganic suspended matter	-
OSM	Organic suspended matter	-
TSM	Total suspended matter (ISM + OSM)	-
U	Current velocity	$m\ s^{-1}$
u	Eastward component of current velocity	$m\ s^{-1}$
v	Northward component of current velocity	$m\ s^{-1}$
w	Vertical component of current velocity	$m\ s^{-1}$
g	Gravitational acceleration	$m\ s^{-2}$
t	Model time step	s
h	Thickness of the model layers	m
Vol	Grid cells volume	m^3
Av_x and Av_y	Horizontal turbulent diffusion coefficients	$m^2\ s^{-1}$
Av_z	Vertical turbulent diffusion coefficient	$m^2\ s^{-1}$
Av_{cur}	Currents component of Av_z	$m^2\ s^{-1}$
Av_{wave}	Waves component of Av_z	$m^2\ s^{-1}$
C	SPM concentration in the water	$kg\ m^{-3} = 10^3\ mg\ l^{-1}$

ρ	Water density	$kg\ m^{-3}$
ρ_{dry}	Dry density of fine sediment	$kg\ m^{-3}$
K_{size}	SPM particle size	m
W_{sink}	Sinking velocity of SPM	$m\ s^{-1}$
C_{sours}	SPM concentration in the sources	$kg\ m^{-3} = 10^3\ mg\ l^{-1}$
C_{sink}	SPM concentration in the sinks	$kg\ m^{-3} = 10^3\ mg\ l^{-1}$
f_{riv}	Percentage of the three SPM fractions in the rivers load	%
L_{riv}	The rivers load of SPM	$kg\ s^{-1}$
D_{riv}	Fresh water discharge	$m^3\ s^{-1}$
C_{riv}	Annual mean SPM concentration in rivers	$kg\ m^{-3} = 10^3\ mg\ l^{-1}$
C_{mean}	Annual mean SPM concentrations in water	$kg\ m^{-3} = 10^3\ mg\ l^{-1}$
C_{max}	Maximum of modeled surface SPM concentration	$kg\ m^{-3} = 10^3\ mg\ l^{-1}$
M_{sed}	Sedimentation mass in the water of SPM per unit area	$kg\ m^{-2}$
C_b	SPM concentration in the bottom water layer	$kg\ m^{-3} = 10^3\ mg\ l^{-1}$
f_{fine}	Content of fine sediment in the seabed	%
f	Percentage of the three SPM fractions in the seabed	%
M	Sediment mass in the seabed per unit area	$kg\ m^{-2}$
Hs	Significant wave height	m
k	Wave number	m^{-1}
T	Peak period	s
U_w	Maximum of the orbital wave velocity	$m\ s^{-1}$
V^*	Shear stress velocity	$m\ s^{-1}$

V^*_{cur}	Currents component of V^*	$m\ s^{-1}$
V^*_{wave}	Waves component of V^*	$m\ s^{-1}$
V^*_{sed}	Threshold value of V^* for sedimentation	$m\ s^{-1}$
V^*_{res}	Threshold value of V^* for resuspension	$m\ s^{-1}$
V^*_{ero}	Threshold value of V^* for erosion	$m\ s^{-1}$
h_{ero}	Depth of erosion	m
k_{ero}	Experimental coefficient, see eq. 2.20	-
V^*_{mean}	Annual mean shear stress velocity	$m\ s^{-1}$
Av_{bio}	Bioturbation coefficient	$m^2\ s^{-1}$
s_f	Season factor of bioturbation	-
l_f	Location factor of bioturbation	-
h_f	Bottom depth factor of bioturbation	-
Av^{max}_{bio}	Maximum of Av_{bio}	$m^2\ s^{-1}$
C^i_A	Analyzed surface SPM concentration field	$kg\ m^{-3} = 10^3\ mg\ l^{-1}$
C^i_P	First-guess SPM concentration field	$kg\ m^{-3} = 10^3\ mg\ l^{-1}$
C^i_O	Observed SPM concentration field	$kg\ m^{-3} = 10^3\ mg\ l^{-1}$
N_{obs}	Number of available observations	-
σ^i_P	Root-mean-square error in the model prediction	-
C^j_T	True value of C	$kg\ m^{-3} = 10^3\ mg\ l^{-1}$
W_{ij}	Weights	-
P	Error correlation matrices of prediction	-
O	Error correlation matrices of observation	-
L_{max}	Radius of influence	-

Bibliography

Asaeda, T. and Wolanski, E. (2002). Settling of muddy marine snow. *Wetlands Ecology and Management*, 10:283–287.

Backhaus, J. (1985). A three-dimensional model for the simulation of shelf sea dynamics. *Dtsch Hydrogr Z*, 38:167–187.

Backhaus, J. and Hainbucher, D. (1987). A finite difference general circulation model for shelf sea and its application to low frequency variability on the north european shelf. In Nihoul, J. and J, B. M., editors, *Three dimensional model of marine and estuarine dynamics*, Elsevier Oceanographic Series, pages 221–244. Elsevier.

Bartels, J. (1957). *Gezeitenkräfte, Handbuch der Physik*, volume II Band XLVIII. Geophysik.

de Swart, H. E. and Calvete, D. (2003). Non-linear response of shoreface-connected sand ridges to interventions. *Ocean Dynamics*, 53:270–277.

der Linde, D. V. (1998). Protocol for total suspended matter estimate. Technical report, JRC Technical Note.

DLR (2007). German aerospace center. Technical report.

DOD (2006). German oceanographic data centre, online dataset, www.bsh.de. Technical report.

Doerfer, R., Schiller, H., and Peters, M. (2006). Meris regional case 2 water algorithms (c2r). http://www.brockmann-consult.de/beam/software/plugins/merisc2r-1.1.zip.

Doerffer, R. and Fischer, J. (1994). Concentrations of chlorophyll, suspended matter and gelbstoff in case-ii waters derived from satellite coastal zone colour scanner data with inverse modeling methods. *J Geoph Res*, 99:745–746.

Dyer, K., Cornelisse, J., Dearnaley, M., Fennessy, M., S.E.Jones, Kappenberg, J., McCave, I., Perjrup, M., andW. van Leussen, W. P., and Wolfstein, K. (1996). A comparison of in situ techniques for estuarine flock settling velocity measurements. *Journal of Sea Research*, 36(1/2):15–29.

Eisma, D. and Kalf, J. (1987). Distribution, organic content and particle size of suspended matter in the North Sea. *Netherlands Journal of Sea Research*, 21 (4):265–285.

Feser, F., Weisse, R., and von Storch, H. (2001). Multi-decadal atmospheric modeling for europe yields multi-purpose data. *EOS Transactions*, 82 28:345–402.

Fettweis, M., Nechad, B., and den Eynde, D. V. (2007). An estimate of the suspended particulate matter (SPM) transport in the southern North Sea using SeaWiFS images, in situ measurements and numerical model results. *Continental Shelf Research*, 27(10-11):1568–1583.

Gayer, G., Dick, S., Pleskachevsky, A., and Rosental, W. (2004). Modellierung von scwebstofftransporten in Nordsee und Ostsee. *Berichte des BSH*, 36.

Gayer, G., Dick, S., Pleskachevsky, A., and Rosenthal, W. (2006). Numerical modeling of suspended matter transport in the North Sea. *Ocean Dynamics*, 56:62–77.

GRDC (2006). Global runoff data centre, online dataset, http://grdc.bafg.de. Technical report.

Günther, H., Hasselmann, S., and Janssen, P. (1992). The wam model cycle 4. Technical report, Deutsches Klimarechenzentrum, Hamburg.

Haarich, M., Kienz, W., Krause, M., and Schmidt, G.-P. Z. D. (1993). Heavy metal distribution in different compartments of the northern North Sea and adjacent areas. *Ocean Dynamics*, 45(5):313–336.

Hirota, J. and Szyper, J. P. (1975). Separation of total particulate carbon into inorganic and organic components. *Limnology and Oceanography*, 20:896–899.

Ilyina, T., Pohlmann, T., Lammel, G., and Suendermann, J. (2006). A fate and transport ocean model for persistent organic pollutants and its application to the North Sea. *Journal of Marine Systems*, 63:1–19.

Jonasz, M. and Fournier, G. R. (2007). *Theoretical and Experimental Foundations Light Scattering by Particles in Water*. Elsevier.

Kochergin, V. (1987). Three-dimensional prognostic models. In Heaps, N., editor, *Three-Dimensional Coastal Ocean Models*, volume 4 of *Coastal and Estuarine Science*, pages 201–208. American Geophysical Union, Washington, DC.

Komen, G., Cavaleri, L., Donelan, M., Hasselmann, K., Hasselmann, S., and P.A.E.M.Janssen (1994). *Dynamics and Modelling of Ocean Waves*. Cambridge University Press.

Krumbein, W. C. and Sloss, L. L. (1963). *Stratigraphy and Sedimentation, 2nd edition*. Freeman, San Francisco.

Lenhart, H. J. and Pohlmann, T. (1997). The ices-boxes approach in relation to results of a north sea circulation model. *Tellus*, 49A:139–160.

Lionello, P. and Günther, H. (1992). Assimilation of altimeter data in a global third-generation wave model. *Journal of geophysical research*, 97(C9):14,453–14,474.

Menzel, D. W. and Ryther, J. H. (1963). The composition of particulate organic matter in the western north atlantic. Technical report, Woods Hole Oceanographic Institution.

Moll, A. (1998). Regional distribution of primary production in the North Sea simulated by a three-dimensional model. *Journal of Marine Systems*, 16:151–170.

National Centers for Environmental Prediction (2005). NOAA - national oceanic and atmospheric administration, NCEP - national centers for environmental prediction. www.noaa.gov.

Nies, H., Harms, I., Karcher, M., Dethleff, D., and Bahe, C. (1999). Anthropogenic radioactivity in the Arctic Ocean - review of the results from the joint german project. *The Science of the Total Environment*, 237(238):181191.

Pätsch, J. and Lenhart, H.-J. (2004). *Daily Loads of Nutrients, Total Alkalinity, Dissolved Inorganic Carbon and Dissolved Organic Carbon of the European continental rivers for the years 1977-2002.*, page 159. Number 48 in Berichte aus dem Zentrum für Meeres- und Klimaforschung, Reihe B: Ozeanographie.

Pleskachevsky, A., Gayer, G., Horstmann, J., and Rosenthal, W. (2005). Synergy of satellite remote sensing and numerical modelling for monitoringof suspended particulate matter. *Ocean Dynamics*, 55(1).

Pleskachevsky, A., Gayer, G., and Rosenthal, W. (2002). Numerical modelling of suspended matter transport. In *11 th International biennial conference on physics of estuaries and coastal seas*, pages 476–479.

Pohlmann, T. (1996). Predicting the thermocline in a circulation model of the North Sea. parti: Model description, calibration, and verification. *Cont Shelf Res*, 7:131–146.

Pohlmann, T. (2006). A meso-scale model of the central and southern North Sea: Consequences of an improved resolution. *Continental Shelf Research*, 26:2367–2385.

Pohlmann, T. and Puls, W. (1994). Currents and transport in water. In Sündermann, J., editor, *Circulation and Contaminant Fluxes in the North Sea*, pages 345–402. Springer Verlag.

Puls, W. (2006). Personal communication.

Puls, W., Kuehl, H., Frohse, A., and Koenig, P. (1995). Measurements of the suspended matter settling velocity in the German Bight (North Sea). *Deutsche Hydrographische Zeitschrift*, 47 (4):259–276.

Puls, W., Pohlmann, T., and Suendermann, J. (1997). Suspended particulate matter in the southern North Sea: Application of a numerical model to extend

NERC North Sea project data interpretation. *German Journal of Hydrography*, 49 Number 2/3:307–327.

Reid, P., Lancelot, C., Gieskes, W., Hagmeier, E., and Weichart, G. (1990). Phytoplankton in the North Sea and its dynamics: A review. *Netherlands Journal of Sea Research*, 26(2-4):295–331.

Rodriguez, I., Alvarez, E., Krohn, E., and Backhaus, J. O. (1991). A midscale tidal analysis of waters around the north western corner of the iberian penninsula. *Proceedings of Computer Model ling in Ocean Engineering*, 91:568.

Simionato, C., Nunez, M., and Engel, M. (2001). The salinity front of the ri'o de la plata - a numerical case study for winter and summer conditions. *Geophysical Research Letters*, 28(13):2641–2644.

Soulsby, R. (1997). *Dynamics of marine sands. A manual for practical application.* Thomas Telford Services, London.

Steele, J. H. and Baird, I. E. (1963). The chlorophyll-a content of particulate organic matter in the northern north sea. Technical report, Marine laboratory, Aberdeen.

Strickland, J. and Parsons, T. (1998). *A practical Handbook of Sea Water Analysis*, chapter 8, pages 181–184. Unipub.

Stronach, J. A., Backhaus, J., and Murty, T. (1993). An update on numerical simulation of oceanographic processes in the waters between vancouver island and the mainland: the gf8 model. *Oceanography and Marine Biology: An annual review*, 31:1–86.

Sündermann, J. and Puls, W. (1990). Modelling of suspended sediment dispersion and related transport of lead in the north sea. *Mitt. Geol.-Paläont. Institut Univ. Hamburg*, 69:143–155.

ten Brummelhuis, P., Vos, R., and Gerritsenb, H. (2001). Skill assessment of SPM transport models using the adjoint technique. *Estuarine, Coastal and Shelf Science*, 53:569–580.

von Storch, H. and Zwiers, W. (1999). *Statistical analysis in climate research*. Cambridge University Press.

WAMDI Group (1988). The WAM Model-A third generation ocean wave prediction model. *Journal of Physical Oceanography*, 18, Issue 12:1775–1810.

Wentworth, C. K. (1922). A scale of grade and class terms for clastic sediments. *Journal of Geology*, 30(9):377–392.

Winterwerp, J., Manning, A., Martens, C., de Mulder, T., and Vanlede, J. (2006). A heuristic formula for turbulence-induced flocculation of cohesive sediment. *Estuarine, Coastal and Shelf Science*, 68(1-2):195–207.

Acknowledgements

First, I thank Dr. Heinz Güunther of GKSS Research Centre for involving me in this interesting project and for his thoughtful support throughout my study.

I would like to acknowledge my supervisor, Prof. Dr. Hans von Storch of GKSS Research Centre and the University of Hamburg for giving me the opportunity to perform this study in the University of Hamburg.

Furthermore I thank P.D. Dr. habil. Thomas Pohlmann of the Institute of Oceanography at the University of Hamburg for providing boundary conditions for HAMSOM and valuable discussions during my study. Many thanks to Dr. Kathrin Wahle and Dr. Roland Doerffer of GKSS for the help in processing of MERIS data; Birgit Gerasch and Dr. Andreas Neumann of DLR for providing MOS data; Stiig Wilkenskjeld of GKSS (now in DMI) for support during the design and multiprocessor optimization of the model code and Dr. Walter Puls of GKSS for the advises regarding the parameterization of vital activity in the seabed. My colleagues Gerhard Gayer, Dr. Andrey Pleskachevsky, Dr. Arno Beherns, Dr. Johan Horstman and Wolfgang Koch from the Data Analysis and Data Assessment Department of the Institute for Coastal Research at the GKSS Research Centre are thanked for the support during my study.

I am grateful to my family and first of all to my wife Dr. Tatjana Ilyina and my son Alexej Dobrynin for the constant support during the whole period I worked on my thesis, as well as to my parents Tatjana and Anatoly Dobrynin for encouraging me.

This study was supported by the Helmholtz-EOS research network of the Helmholtz Association.